

## #1 Review for WCD-2020-1, Revision 1 (RC1 from 01 June 2020)

### General Comments

The changes and additions made by the authors have further improved what was already a very good piece of work. However, reading the revised manuscript I felt that the text could be improved in a number of ways. I have tried to cover these in my suggestions below, but I would encourage all co-authors to give the paper a thorough read through before the final submission to make sure that things are clearly explained, particularly when it comes to the methodology. I also have a concern regarding the use of the word “triggering” to describe the role of cut-off lows and PV filaments in the event, which I believe needs to be addressed. As such I am recommending further minor revisions.

### Specific Comments

My only significant comment relates to your repeated use of the word “triggering” to describe the role of the cut-off lows and PV filaments in this event. In general, convective triggering refers to the process whereby air parcels are lifted to their level of free convection and subsequently rise through buoyant accelerations. For an individual convective cell (thunderstorm) this process occurs on the scale of a few kilometres to ~100 km (i.e. the meso- $\beta$  or meso- $\gamma$  scale following Orlanski 1975; see also Markowski and Richardson 2010, section 1.1). On the other hand, lifting associated with cut-off lows and other synoptic-scale disturbances occurs on length scales of 100 s of kilometres to ~1000 km (meso- $\alpha$  scale). It is generally accepted that this lifting contributes indirectly to convective initiation (triggering) through the generation of CAPE and the removal of CIN, via changes in lapse rate (see Markowski and Richardson 2010, section 7.1) - in other words large-scale ascent primes the atmosphere for convective initiation. However, the initiation process itself is typically associated with phenomena such as convergence lines, thermally driven circulations (sea/lake/vegetation breezes), orographic lifting, and boundary-layer thermals, at least for surface-based convection (some elevated MCSs may be directly triggered by large-scale ascent). I think it is important that this distinction is clearly articulated in your paper. As such you need to modify the text in several places, including L56-59, L425, L433-434, L460-462, and L584.

AC: We followed this recommendation, delete the word “trigger” and modified all sentence in the lines mentioned. For example, we explained in Sect. 5 that large-scale lifting provides weak yet persistent ascent, which serve to precondition the thermodynamic environment via adiabatic cooling and thus increase in CAPE and reduction in CIN.

L27-34: You should restructure this part of the paragraph so that the three ingredients for deep moist convection are listed together. State the ingredients first and then discuss the scale of the processes they are associated with (synoptic for instability and moisture; mesoscale to storm scale for the lifting mechanism).

AC: We changed this as desired. “In general, the development of convective storms results from scale interactions of different processes in the atmosphere. It is well known that deep moist convection depends on three necessary but not sufficient ingredients: (i) convective instability over a layer of sufficient depth, (ii) sufficient moisture in the lower troposphere and (iii) a suitable lifting mechanism for the triggering of convection. The first two requirements are usually controlled by processes on the synoptic scale. The latter one can occur at different scale ranges.”

L31: Latent and conditional instability are one and the same (see, for example, [http://glossary.ametsoc.org/wiki/Latent\\_instability](http://glossary.ametsoc.org/wiki/Latent_instability)). Also, potential instability is generally not considered to be a major factor in the preconditioning of convective environments (see section 3.1.3 of Markowski and Richardson 2010). There are also various other forms of instability (centrifugal, inertial, symmetric, shear). As such I would just state conditional instability as the first of the three ingredients for deep, moist convection.

AC: We changed the sentence by deleting the parenthesis with “conditional, latent, potential” to “(i) convective instability over a layer of sufficient depth and (ii)...”

L62: It should be “fully” not “full” here. However, I would actually recommend deleting this sentence as it is a bit “hand wavy”.

AC: That’s right. Thanks for the careful reading. However, as suggested, we now deleted the sentence.

L78: I would say “mesoscale cut-off lows and PV filaments”.

AC: We deleted one meso-scale.

L82: Get rid of “and their accompanying phenomena”

AC: We deleted this part.

L84: “prior to”

AC: Thanks for the careful reading.

L87: Get rid of “The next” and add “then” after “Section 4” (i.e. “Section 4 then puts the results in a historical context”)

AC: We changed this.

L94: Rather than “secondary effects” I would say “associated hazards”.

AC: We changed this.

L103: You need to say “allow us to investigate” or, alternatively, “permit/facilitate an investigation of”.

AC: Thanks for the careful reading.

L126: I think it should just be “Météo-France”, not “the Météo-France”.

AC: Thanks for the careful reading.

L128-129: Here and elsewhere I would use the term “1-hour extreme rainfall events” rather than “hourly extreme rainfall events”. Generally, I would take “hourly” to mean “occurring every hour” rather than “lasting for 1 hour”. This is also consistent with “3-hour extreme rainfall events”.

AC: We added this suggestion.

L135: Since “the RR collective” isn’t mentioned again, you can get rid of the statement in parentheses.

AC: We changed this.

L147: “location and scale parameters, respectively”

AC: We added this suggestion.

L150: I think you mean “standard deviation” not “derivation”

AC: Thanks for the careful reading.

L152: You can either just say “return period” here or use the symbol  $t_{RP}$ ; you don’t need both as this definition is already given in the previous sentence.

AC: We added this suggestion.

L158: Suggest changing to “12 equidistant vertical levels extending from 1 km to 12 km above ground level (AGL)”.

AC: We added this suggestion.

L169-170: I’m not sure it is fair to assume weaker cells “cannot move at higher speeds” than those above 55 dBZ. I would instead simply note the caveat that your use of a high reflectivity threshold means that the resulting storm-motion estimates may not be representative of weaker convective cells.

AC: We modified the sentence: “Even if weaker cells are not detected using the 55 dBZ thresholds, it can be assumed (cf. Video Supplement for two representative days) that they cannot move with higher speeds.”

L189-190: Suggest modifying the end of this sentence as follows: “...to describe the large-scale meteorological conditions and define weather regimes (see Sect. 2.3), perform kinematic backward trajectories (see Sect. 2.4), and identify cut-off lows (see Sect. 2.5).”

AC: We added the suggestion.

L193: Here and throughout your analysis you should say “bulk wind difference (BWD)” rather than “bulk wind shear”. Shear has units of  $s^{-1}$  as it is the BWD divided by the layer depth.

AC: Basically this is right. But in the literature, such as in Weisman and Klemp (1982), Bunkers (2002), Markowsky and Richardson (2010), or Trapp (2013), the wind difference is termed to as “vertical wind shear”, even though it does not have units of shear.

Bunkers, M. J. (2002): Vertical wind shear associated with left-moving supercells. *Weather Forecast.*, 17, 845-855, [https://doi.org/10.1175/1520-0434\(2002\)017<0845:VWSAWL>2.0.CO;2](https://doi.org/10.1175/1520-0434(2002)017<0845:VWSAWL>2.0.CO;2).

L198: Rather than using Z500' for 500 hPa geopotential height anomalies, I suggest using Z500 to represent 500 hPa geopotential height and explicitly stating when you are talking about an anomaly. For example, on L206 you would say “dominated by a negative Z500 anomaly”.

We changed this as desired.

L199: Why did you choose the first seven EOFs? What percentage of the total variance do they collectively explain?

AC: Following other work, e.g. Ferranti et al. 2015, we opted for the minimum number of EOFs explaining more than 75 % of the total variance, which for the normalised Z500 was seven and the total variance explained then is 76,7 %. See for details Grams et al. (2017).

L217-218: Presumably, the five “surrounding” grid points are the nearest grid point to the sounding site and its immediate neighbours to the north, south, east and west; however, this should be stated explicitly.

AC: We added the suggestion.

L220: Get rid of “where the air masses relevant for the thunderstorm development are located”. Air below 950 hPa and above 600 hPa is certainly relevant for thunderstorms!

AC: We deleted this part.

L224: Rather than “the literature” I would say “previous studies” (or work or research).

AC: We added the suggestion.

L245-257: This description of the persistence analysis is quite difficult to follow, particularly the first paragraph. As such I would recommend completely rewriting it. Also, as stated in my original review, you should avoid using the term “cluster” here (and in Fig. 15) to avoid confusion with the actual cluster analysis used to define weather regimes.

AC: We revised the paragraph and hope that the method is now clearer and easier to understand.

Furthermore, we also reduced the word cluster even more.

L257: What do you mean by “the maximum of the daily minima”? Please rephrase.

AC: We deleted the sentence, since the thresholds are defined and used (as already described) in PIP16.

And the interested reader is referred to the study.

L268: Get rid of “an area” before “twice the size of Germany”

AC: We added the suggestion.

L275: I think you mean “evolution” rather than “evaluation” here.

AC: Thanks for the careful reading.

L285: What does “(radar visibility)” indicate? Are you saying that the cells were only visible on radar for 30 minutes? Please explain or delete this if isn't important.

AC: It is important to mention because the radar visibility is shorter than the lifetime of the cell; we changed “(radar visibility, i.e., period of precipitation)”

L290: As stated in my original review, you should avoid using parentheses to save space as the resulting sentences are much more difficult to read and comprehend.

AC: We changed this as desired.

L312: This sentence has some grammatical errors. I suggest revising as follows: “However, this rain fell in a period of 3 hours, with 60 mm falling in just 50 min.”

AC: Thanks for the careful reading. We changed this as suggested.

L320: Put “indicating wind speeds between 25 and 31 m/s” in parentheses.

AC: We changed this as desired.

L324-327: This sentence would also benefit from rewording. Something like “In a few cases, deep-layer shear magnitudes were sufficient (BWD up to 20 m/s) for the development of severe storms, with large hail up to 5 cm in diameter recorded in Southwest France on 26 and 9 June and in southern Germany on 11 June.”

AC: Thanks for the suggestion; we changed the sentence.

L359: “(Fig. 6a)”

AC: We added this.

L367: Why introduce the abbreviations “ZO” and “EuBL” here if you aren’t going to use them in the text?

AC: To make the connection to the figure quicker and easier.

L379: I would say “a pronounced decrease in convective activity”

AC: We changed this as desired.

L385: Get rid of the first instance of “values”

AC: We changed this.

L396: Since your analysis considers geopotential height on constant pressure surfaces you should say “weak geopotential height gradients”.

AC: We changed this as desired.

L403: One way to highlight the strong relationship between V500 and BWD would be to compute the correlation coefficient between the two. You could do this both for the sounding data and the ECMWF analysis over the domain shown in Fig. 8. Just a thought.

AC: This is a nice thought; however, the two figures already indicate similar conditions and the key message will not change.

L405: Get rid of “squall lines” (MCS covers this).

AC: We deleted this part.

L407: Not sure what you mean by deep-layer shear. In my experience this is another name for the 0-6 km (or surface-500 hPa) BWD. As noted above, shear has units of  $s^{-1}$ , not  $m s^{-1}$ .

AC: We modified the sentence. BWS represents the directional shear; here, we mean the speed shear (difference between two wind speed values). Regarding the units see answer above.

L409-422: I recommend using the term “air parcels” rather than “air masses” in this section, since the former is more consistent with what a back trajectory represents.

AC: Basically this is right. But, when we are talking in the section about “air mass”, we already mean/associate the whole.

L469-470: Suggest rewording this sentence as follows: “This analysis is restricted to Germany due to the availability of long-term (> 50 years), high-resolution (1 km<sup>2</sup>) gridded rainfall data.”

AC: We changed this as suggested.

L479: What do you mean by “partly with new all-year records”? Maybe rephrase this.

AC: We deleted the sentence.

L480-481: Suggest rewording this sentence and connecting it with the next one (getting rid of the paragraph break in the process) as follows: “This does not appear to be an artefact of insufficient gauge density, as most events are represented by multiple gauges (not shown). Instead, it likely reflects the very

slow propagation of storms...”

AC: We changed this as suggested.

L493-494: Suggest getting rid of (or moving) the sentence beginning “Recall that” as it breaks up the flow between the preceding and following sentences. Also, in the next sentence, suggest changing “In doing so” to “Thus”.

AC: We moved the sentence and added the second suggestion.

L504: Here and elsewhere in this section, change “event persistence(s)” to “CE duration”.

AC: We added the suggestion.

L508-509: Change “event persistences of CE with long duration” to “long-duration CEs”.

You might consider completely rewording this sentence as follows: “To put these numbers in context, Fig. 15 shows the relative frequency of CEs in May/June as a function of their duration for the period 1981 to 2010.”

AC: We changed the formulation as suggested.

L510-515: This additional explanation of the procedure is confusing and unnecessary. I recommend getting rid of it and the subsequent paragraph break.

AC: This addition was made at the request of the second reviewer after the first draft. It is important to note how the relative frequency is calculated in case someone wants to repeat the procedure.

L541: Change “convective” to “convection”

AC: Thanks for the careful reading.

L581: Change “due to several reason” to “in several respects”

AC: We added the suggestion.

L611: I’m not sure what you mean by “(e.g. jet stream)”. Please either elaborate or delete this.

AC: We deleted this comment.

Table 1: I don’t think the track length and area are particularly informative, so these can probably be removed. The information on rainfall intensity and storm speed are more useful, but you don’t actually discuss them anywhere in the text.

AC: We have already mentioned the information on rainfall intensity, track length, and propagation speed in the last draft in connection with the discussion of the station Bruchweiler (Vers 2: Line 311–314; now Line 311–316) and the station Diethenhofen (a few lines later).

Now, we deleted the total track area in Table 1. Concerning the track length, we added a further comment in conjunction with Figure 4.

Figure 2: Rather than saying “the extended study period” I would give the dates explicitly (i.e. 1 May to 20 June).

AC: We added the information.

Figure 3: What do you mean by “total maximum”?

AC: We deleted “total”. We mean the maximum during the study period (as already described).

Also, as stated in my original review you should say “accumulation” rather than “sum” when referring to rainfall amounts in mm.

AC: We changed this.

Figure 4: I don’t think it is necessary or appropriate to apply a spline filter to the distributions here. Just plot the raw data as histograms (c.f. Fig. 11).

AC: We plotted the raw data in Figure 4 without spline interpolation.

Figure 6: For some reason your color bars have more ticks than colours. Also the number of ticks per color varies and the tick labels don’t always align with changes in the color level. Please make it so that the ticks and labels occur at the boundaries between the colors; otherwise it is difficult for the reader to extract

quantitative information from the figure. The caption for this figure also needs revising for clarity. Here is my suggestions: “Mean anomalies during May/June 2018 of (a) 500 geopotential height anomaly (shaded in gpm) and (b) integrated water vapour anomaly (shaded in  $\text{kg m}^{-2}$ ), together with the mean 500 hPa geopotential height (contours every 40 gpm). Data are from ERA-Interim and anomalies are computed with respect to the 1981-2010 climatology.”

AC: We corrected the figure legend and revised the caption according the suggestion.

Figure 7: Panel (a) needs to be better explained in the caption. In particular, you should state the meaning of the bold sections of the curves and the colours along the x axis. Also, in panel (c) the y axis should be labelled as “V500 (m/s)”.

AC: We revised the caption, which now explains clearer the meaning of weather regime life cycles.

Figure 8: Add “at 12 UTC” before “averaged over the study period” and get rid of “12 UTC” from the parentheses at the end.

AC: We changed this.

Figure 9: Please explain either in the caption or the main text how the ellipses were defined. Also, I suggest using “distance along trajectory” instead of “total distance”.

AC: We included such an explanation in the caption of Figure 9. The axis label in panel (b) has been changed accordingly.

Figure 13: Change “Return periods” to “Return period” (singular).

AC: We changed this.

Figure 14: I think you mean “2nd and 3rd quartiles” (not “1st and 3rd”).

AC: No; we mean the 1<sup>st</sup> and 3<sup>rd</sup> quartiles. 1<sup>st</sup> (lower) = 25 %; 2<sup>nd</sup> = 50 % = Median; 3<sup>rd</sup> (upper) = 75 %.

Also, I would recommend making the whiskers and outliers the same colour as the boxes and using solid rather than dashed lines for the whiskers.

AC: The software that was used to produce the figure unfortunately does not support this.

Figure 15: As noted above (and in my original review) you should avoid using the term “cluster” in this analysis. Instead I recommend using “CE duration” (this should also replace “event persistence”).

AC: We adapted this.

Also, it should be “May”, not “Mai”.

AC: Thanks for the careful reading

Figure 16: I believe this information could be better presented in Fig. 10, by replacing the Z500 contours (which are already shown in Fig. 6) with the climatological cut-off low frequency. This way the reader can directly compare the climatological and 2018 cut-off low frequencies without the need to consider anomalies of percentages. You can then get rid of Fig. 16.

AC: In addition to a parallel presentation of Z500 and the cut-off frequency (Fig. 10) for easier comparison, we also want to show the cut-off anomaly (study period vs. climatology; even if it looks quite similar); however, we combined Figure 10 and 16 into Figure 10a and 10b, so that the aspect of comparability is better considered.

## #2 Review for WCD-2020-1 Revision 2 (RC2 from 05 June 2020)

The paper describes an extraordinary thunderstorm episode of western and central Europe in May/June 2018. The situation was related to an unusually high cut-off low activity at the upstream side of a quasi-stationary blocking. The authors use multiple data sets to study the situation. The paper improved highly from the first version: It is now an easy, nice read. The paper has a very good, easy-to-follow structure. An additional trajectory analysis gives insight to the quasi-stationarity of the situation. An interesting outcome is the potential linkage between large-scale weather patterns (European weather regimes) and thunderstorm activity which should be studied in more detail in the future.

AC: Thanks. The latter point is already the plan for further investigations :)

Abstract: I like the abstract. I think an additional last sentence would be nice that describes the benefits and aim of the paper. Something like you write in line 76-80 in your introduction:

"The primary objective of this paper is to examine the conditions and processes that made this particular thunderstorm episode in 2018 unique. We focus on the process interaction across scales, i.e., from the large-scale dynamics such as atmospheric blocking to meso-scale PV cut-off lows and/or small meso-scale PV filaments to modifications of the convective environment to local-scale thunderstorm occurrences. Further objectives are to highlight the synoptic setting during the thunderstorm episode, to demonstrate the severity of the events, and to place the event in a historical context."

AC: Thanks. We added one sentence about the objectives.

### More specific comments:

2. Data and Method: This section improved really much. It is now very clear what kind of data you use for what purpose. And it gives a clear and concise overview. Thanks for taking into account the reviewer's comments!

AC: There were also good comments.

Section 3.1.1: I like the connection the authors made between regime changes and convective activity. This would be interesting for a future climatology!

AC: That is already the plan for further investigations :)

Section 3.1.2: Thanks for adding a comparison with bulk wind shear. The comparison nicely shows that V500 is almost identical to BWS over land in this situation. Overall the unusual situation seems to be clearer discussed (or plotted)

AC: Thanks.

Section 3.2: Thanks for adding the trajectory analysis. It is a nice addition. Especially the length of track vs. ellipse size

AC: Thanks.

Section 3.3: This is probably my only real CRITIQUE here: You discuss cut-off low C3 being responsible for the thunderstorm activity over southeast Germany, central France and the Netherlands. However, from your figure 5e it rather seems to be cut-off low C1. The cut-off low detection method seems to join the several smaller cut-offs or filaments. However, the center of C3 is still over the Atlantic Ocean? I would at least write a clear comment here or rename the identified cut-off low blob in Fig 12. In my opinion, C3 is just embedded in a larger scale system - and so is C1 (which seems to be rather associated with the thunderstorms).

AC: The reviewer is absolutely right; the way we wrote it, it sounds like C3 was responsible for the thunderstorm activity over southeast Germany, central France and the Netherlands (but we only meant that the trough arrived from the Atlantic with C3). However, C1 is responsible for this. We modified the text in Sect. 3.3 for clarification and added a reference in section 3.1 in the context of C1 (line 349).

Thanks for the careful reading!

5. Discussion: lines 540-541: "Interestingly, atmospheric blocking was key to providing the large-scale setting conducive for convective in its vicinity." - There seems to be a word missing after convective?

AC: We mean "convection". Thanks for the careful reading.

6. Summary and Conclusions: line 584: "(iii) the large cut-off low frequency that was responsible for the majority of convection triggering" - I would rather say "associated with" instead of "was responsible for", because: Could you really prove that the cut-off lows were responsible?

AC: That's right. We changed this. Thanks for the suggestion.

Fig. 5: I like the blue dots! It would be good to comment on the dots in the main text as well!

AC: We added some words in Sect. 3.1. (line 352)

Overall, the quality of the figures is good.

# The role of large-scale dynamics in an exceptional sequence of severe thunderstorms in Europe May/June 2018

Susanna Mohr<sup>1</sup>, Jannik Wilhelm<sup>1</sup>, Jan Wandel<sup>1</sup>, Michael Kunz<sup>1,2</sup>, Raphael Portmann<sup>3</sup>, Heinz Jürgen Punge<sup>1</sup>, Manuel Schmidberger<sup>1</sup>, Julian F. Quinting<sup>1</sup>, and Christian M. Grams<sup>1</sup>

<sup>1</sup>Karlsruhe Institute of Technology (KIT), Institute of Meteorology and Climate Research (IMK), Karlsruhe, Germany

<sup>2</sup>Center for Disaster Management and Risk Reduction Technology (CEDIM), Karlsruhe, Germany

<sup>3</sup>Institute for Atmospheric and Climate Science, ETH Zurich, Switzerland

**Correspondence:** Susanna Mohr (mohr@kit.edu)

1 **Abstract.** Over three weeks in May and June 2018, an exceptionally large number of thunderstorms hit vast parts of western  
2 and central Europe, causing precipitation of up to 80 mm within one hour and several flash floods. **This study examines**  
3 **the conditions and processes that made this particular thunderstorm episode exceptional. Besides a description of the**  
4 **synoptic setting and the severity of the convective hazards, it is shown how processes interact across scales, from large-**  
5 **scale dynamics with atmospheric blocking to meso-scale cut-off lows to regional convective environment to local-scale**  
6 **thunderstorm occurrences.**

7 **During the episode, a blocking situation persisted over northern Europe.** Initially, the southwesterly flow on the west-  
8 ern flank of the blocking anticyclone induced the advection of warm, moist, and unstably stratified air masses. Due to the  
9 low-pressure gradient associated with the blocking anticyclone, these air masses were trapped in western and central Europe,  
10 remained almost stationary and prevented a significant air mass exchange. In addition, the **weak geopotential height gra-**  
11 **dients** led to predominantly weak flow conditions in the mid-troposphere and thus to low vertical wind shear that prevented  
12 thunderstorms from developing into severe organized systems. Due to a weak propagation speed in combination with high rain  
13 rates, several thunderstorms were able to **accumulate enormous amounts of precipitation** that affected local-scale areas and  
14 triggered several torrential flash floods.

15 Atmospheric blocking also increased the upper-level cut-off low frequency on its upstream regions, which was up to 10  
16 times higher than the climatological mean. Together with filaments of positive potential vorticity (PV), the cut-offs provided  
17 the meso-scale setting for the development of a large number of thunderstorms. During the 22-day study period, more than  
18 50 % of lightning strikes can be linked to a nearby cut-off low or PV filament. The exceptionally persistent low stability over  
19 three weeks combined with a weak wind speed in the mid-troposphere has not been observed during the past 30 years.

20 **Keywords:** Europe, thunderstorms, severe convective storms, heavy rain, flash floods, atmospheric blocking, weather regimes, cut-off lows, potential vorticity

## 21 1 Introduction

22 Historically, the period from May to mid of June 2018 was among the most active periods of severe convective storms associated  
23 with heavy rain, hail, convective wind gusts and even tornadoes over large parts of western and central Europe (WetterOnline,  
24 2018a, b, c; DWD, 2018a). More than 1,500 reports of hazardous weather events were documented by the European Severe  
25 Weather Database (ESWD; Dotzek et al., 2009). Rainfall totals of up to 90 mm within a few hours caused (pluvial) flash floods  
26 in various municipalities. Gust speeds of up to  $30 \text{ m s}^{-1}$  led to numerous fallen trees and severely damaged buildings. For  
27 example, from 26 May to 1 June 2018, thunderstorms caused insured losses of about 300 million USD and overall losses of  
28 about 430 millions USD according to Munich Re's NatCatSERVICE (Munich Re, 2019). Thus, it was the costliest convective  
29 storm event in western Europe that year.

30 In general, the development of convective storms results from scale interactions of different processes in the atmosphere. It is  
31 well known that deep moist convection depends on three necessary but not sufficient ingredients (e.g. Johns and Doswell, 1992;  
32 Trapp, 2013): (i) **convective instability over a layer of sufficient depth, (ii) sufficient moisture in the lower troposphere,**  
33 **and (iii) a suitable lifting mechanism for the triggering of convection. The first two requirements are usually controlled**  
34 **by processes on the synoptic scale. The latter** can occur at different scale ranges. For example, lifting mechanisms on the  
35 mesoscale include orographic lifting, horizontal convective rolls, or gravity waves (e.g. Wilson and Schreiber, 1986; Browning  
36 et al., 2007; Barthlott et al., 2010), whereas large-scale lifting can be related to drylines or cold fronts (e.g. Bennett et al., 2006;  
37 Kunz et al., 2020). A further relevant condition for the evolution of deep moist convection is the vertical wind shear, which is  
38 decisive not only for the organizational form, the longevity and thus the severity of the convective storms (e.g. Weisman and  
39 Klemp, 1982; Thompson et al., 2007; Dennis and Kumjian, 2017), but also for their propagation (Corfidi, 2003).

40 The general synoptic situation during the thunderstorm episode 2018 investigated in this study was similar to that prevailing  
41 over a 15-day period in May/June 2016, where also an exceptionally large number of thunderstorms caused several flash floods,  
42 primarily in Germany (Piper et al., 2016; Bronstert et al., 2018; Ozturk et al., 2018). During the episode in 2016, a blocking  
43 anticyclone over the North Sea and Scandinavian region prevented an exchange of the dominant unstably stratified air masses  
44 over several days. In addition, low wind speeds throughout the troposphere caused the thunderstorms to be almost stationary  
45 with the effect of torrential rain accumulations in several small regions (Piper et al., 2016, hereinafter referred to as PIP16).

46 Atmospheric blocking, with a typical lifetime of several days to weeks, is a quasi-stationary, persistent flow situation that  
47 modulates the large-scale extratropical circulation (Rex, 1950a, b; Barriopedro et al., 2006; Woollings et al., 2018). Such  
48 blocks typically occur either in a *dipole configuration* with an accompanying cut-off low on the equatorward side (Rex, 1950a;  
49 Tibaldi and Molteni, 1990) or they adopt an *omega-shape* with cut-off lows forming at the flanks of the blocked region (Dole  
50 and Gordon, 1983). In the potential vorticity (PV) framework, a cut-off low is an upper-level closed anomaly of stratospheric  
51 high PV air (e.g. Wernli and Sprenger, 2007; Nieto et al., 2007a, 2008). PV anomalies, in general, have a far-field impact  
52 on the meteorological conditions in their surroundings (cf. Hoskins et al., 1985). Below the positive PV anomaly, isentropes  
53 bend upward, resulting in reduced static stability and increased lifting. Due to an induced cyclonic circulation anomaly, the  
54 positive PV anomaly favours isentropic gliding up and thus ascent along the isentropes that usually bend upward towards the

55 pole. Finally, when the positive PV anomaly propagates, air masses ascend isentropically at the PV anomalies' upstream side.  
56 These three mechanisms associated with lifting are intrinsic to upper-level positive PV anomalies in general. Additionally, at  
57 the flanks of a mature PV cut-off, small meso-scale filaments of positive PV often separate and are advected away, particularly  
58 when the PV cut-off gradually decays (Portmann et al., 2018). When such a positive PV filament moves over air masses  
59 that are conditionally or potentially unstably stratified, **the associated lifting indirectly contributes to convective initiation**  
60 **(triggering) and thus – if the air parcel reaches its level of free convection – to release of Convective Available Potential**  
61 **Energy (CAPE) and to removal of Convective Inhibition (CIN).** The effect of large-scale PV anomalies accompanied by  
62 cut-off lows on deep moist convection (in relation to severe precipitation events) has already been observed in other studies  
63 showing for Europe that this is an important mechanism for convection due to the associated patterns of advection and vertical  
64 motion (Roberts, 2000; Morcrette et al., 2007; Browning et al., 2007; Russell et al., 2012). ~~But the effect is complex and not~~  
65 ~~fully understood.~~

66 At first, atmospheric blocking was primarily known for its conjunction to extreme weather events such as cold spells and  
67 heatwaves (and associated droughts; e.g. Pfahl and Wernli, 2012a; Bieli et al., 2015; Schaller et al., 2018; Röthlisberger and  
68 Martius, 2019). But in peripheral locations upstream and downstream of the blocks can also create environmental conditions  
69 conducive for deep moist convection development. Thus, the link to heavy precipitation events (including flood events) has  
70 already been intensively investigated in past years (e.g. Martius et al., 2013; Grams et al., 2014; Piaget et al., 2015; Sousa et al.,  
71 2017; Lenggenhager et al., 2018; Lenggenhager and Martius, 2019). A new study by Mohr et al. (2019) now shows a statistical  
72 relationship between convective activity (based on lightning data) and specific blocking situations in the European sector. They  
73 found a block over the Baltic Sea frequently associated with increased thunderstorm occurrences because of southwesterly  
74 advection of warm, moist and unstable air masses on its western flank. In addition, such situations are usually associated with  
75 weak wind speed at mid-tropospheric levels and thus weak vertical wind shear over the thunderstorm area with the consequence  
76 that thunderstorms become often stationary and rarely develop into large organized convective systems. Recently, Tarabukina  
77 et al. (2019) also demonstrate a correlation between the annual variation of summer lightning activity in Yakutia (Russia) and  
78 the frequency of atmospheric blocking in Western Siberia.

79 The primary objective of this paper is to examine the conditions and processes that made this particular thunderstorm episode  
80 in 2018 unique. We focus on the process interaction across scales, i.e. from the large-scale dynamics such as atmospheric  
81 blocking to meso-scale PV cut-off lows and small meso-scale PV filaments to modifications of the convective environment to  
82 local-scale thunderstorm occurrences. Further objectives are to highlight the synoptic setting during the thunderstorm episode,  
83 to demonstrate the severity of the events, and to place the event in a historical context.

84 The paper is structured as follows: Section 2 presents the different data sets and the methods used. Section 3 starts with a  
85 description of the thunderstorm episode in 2018 ~~and their accompanying phenomena~~ by investigating different observation data  
86 such as lightning information, hazardous storm reports, rain gauge measurements, and radar-based storm tracks estimating the  
87 propagation speed. Subsequently, the synoptic situation prior **to** and during the examined thunderstorm episode is investigated  
88 by analyses of the large-scale flow situation, backward trajectories, accompanied weather regimes, and environmental condi-  
89 tions such as instability, moisture, or mid-tropospheric wind speed. Furthermore, we examine the role of PV cut-off and PV

90 filaments on the development of deep moist convection. **Then**, Section 4 puts the results in a historical context, whereby the  
91 exceptional nature of the thunderstorm episode is assessed by relating the observed rainfall totals, the prevailing environmen-  
92 tal conditions, and the occurrence of cut-off systems to long-term data records. Finally, Section 5 and Section 6 discuss and  
93 summarize the main results and draw conclusions.

## 94 **2 Data and methods**

95 The study area includes parts of central and western Europe – France, Benelux (Belgium, Netherlands, Luxembourg), Germany,  
96 Switzerland and Austria (see Fig. 1). The study period extends over three weeks from 22 May to 12 June 2018, where most of  
97 the thunderstorms and **associated hazard** such as heavy rain, hail and convective wind gusts occurred (see Sect. 3). To highlight  
98 the synoptic situation prior to the episode and to emphasise that severe convection during the study period was embedded in  
99 a longer lasting unusual large-scale flow situation, we considered an extended study period from 1 May to 20 June 2018. For  
100 the purpose of climatological comparison, the 30-year period from 1981 to 2010 (1 May to 30 June) was the reference period  
101 (unless otherwise indicated).

### 102 **2.1 Observation data**

103 For the description of the thunderstorm episode in 2018, we use different observation data. Lightning data offer the best  
104 spatially homogeneous coverage for a complete thunderstorm detection, but does not discern according to severity. For this  
105 purpose, we use eyewitness reports of the ESWD and precipitation observations (station-based and gridded-based). Radar-  
106 based storm tracks **permit an investigation of** the propagation speed of the convective cells. Some investigations are limited  
107 to Germany, for which data were available (storm tracks, REGNIE), but enable a deeper insight into the exceptional nature of  
108 the phenomena. Additionally, the atmospheric conditions are examined with data from various sounding stations. Some data  
109 records are also available consistently and homogeneously over long-term periods, which allow us to compare the episode with  
110 historical conditions/events.

#### 111 **2.1.1 Lightning data**

112 Lightning data are obtained from the ground-based low-frequency lightning detection system operated by Siemens as part of  
113 the EUCLID network (EUropean Cooperation for LIghtning Detection; Drüe et al., 2007; Schulz et al., 2016; Poelman et al.,  
114 2016). Available for the whole study domain, the data are projected on an equidistant grid of  $10 \times 10 \text{ km}^2$  and accumulated  
115 over 6-hour periods centered around the timesteps in ERA-Interim (e.g. for the 06 UTC reanalysis the lightning period is  
116 03–09 UTC). This allows the data to be linked to the cut-off lows (see Sect. 2.5). We consider all types of flashes including  
117 cloud-to-ground, cloud-to-cloud, and intra-cloud flashes, whereas polarity or peak current are not investigated.

## 118 2.1.2 ESWD reports

119 We use reports of heavy rain, hail (diameter  $\geq 2$  cm), and convective wind gusts  $\geq 25$  m s<sup>-1</sup> from the European Severe Weather  
120 Database (ESWD; Dotzek et al., 2009; Groenemeijer et al., 2017). The ESWD is a step-by-step quality controlled (four levels)  
121 database providing detailed information about severe convective storms in Europe, mainly based on reports from storm chasers,  
122 eyewitnesses, voluntary observers, meteorological services, and news media. We consider all records with a quality level QC0+  
123 and above. Using a homogeneous data format, these observations contain information about hazardous weather events such as  
124 location, time, intensity, and damage-related information. For a detailed description of the event reporting criteria see ESSL  
125 (2014).

## 126 2.1.3 Rainfall totals

127 Daily rainfall totals of 232 stations distributed across the domain (41°N – 58°N, 4°W – 20°E) were collected from the European  
128 Climate Assessment and Dataset (ECA&D), a database of daily meteorological station observations across Europe (Klein Tank  
129 et al., 2002). In addition, hourly and daily data were obtained from the Météo-France (1223/1935 stations with hourly/daily  
130 data), the Royal Netherlands Meteorological Institute (KNMI; 50/322), the German Weather Service (DWD; 958/810), Me-  
131 teoSwiss (952/0), and the Central Institution for Meteorology and Geodynamics (ZAMG; 254/0). For statistics of **1-hour** and  
132 3-hour extreme rainfall events, we applied the same severity thresholds used in the ESWD (ESSL, 2014), which amount to 35  
133 and 60 mm, respectively (Wussow, 1922; Nachtnebel, 2003). Note that the 24-hour criterion of 170 mm was not measured at  
134 any of the stations.

135 Statistical return periods of single heavy precipitation events are estimated using regionalized precipitation data (*REGion-*  
136 *alisierte NIEderschläge*, REGNIE) provided by DWD (DWD, 2018b). REGNIE is a gridded data set of 24-hour totals (from  
137 06 UTC to 06 UTC on the next day) based on approximately 2,000 climate stations more or less evenly distributed across  
138 Germany (the so-called RR-collective). The REGNIE algorithm interpolates the measurement data to a regular grid of 1 km<sup>2</sup>  
139 considering altitude, exposure, and climatology (Rauthe et al., 2013). The data covering only Germany are available since  
140 1951. The long-term availability of REGNIE over almost 70 years is the decisive advantage compared to other data sets such  
141 as RADOLAN (merger between radar and station data; DWD, 2019), which have a higher spatial and temporal resolution but  
142 are only available for 20 years. Note that the REGNIE time series are affected by temporal changes in the number of rain  
143 gauges considered by the regionalization (Rauthe et al., 2013). For our purpose, the homogeneity of the data are sufficient.

144 Statistical return periods of REGNIE totals are quantified using the Generalized Extreme Value (GEV) distribution (e.g.  
145 van den Besselaar et al., 2013; Ehmele and Kunz, 2019). The Fisher-Tippett Type I distribution, also known as the Gumbel  
146 distribution (Gumbel, 1958; Wilks, 2006), has been extensively used in various fields including hydrology for modelling  
147 extreme events, i.e. to estimate statistical return periods or return values (Sivapalan and Blöschl, 1998; Rasmussen and Gautam,  
148 2003). The Gumbel cumulative distribution function (CDF) for the precipitation totals  $R$  is given by:

$$149 F(R) = \exp \left[ - \exp \left( \frac{\zeta - R}{\beta} \right) \right], \quad (1)$$

150 with  $\zeta$  and  $\beta$  as location and scale parameters, **respectively**. For their estimation, we use the Method of Moments (Wilks, 2006,  
151 Chap. 4) and considered the 67-year period from 1951 to 2017 (summer half-year from April to September):

$$152 \quad \beta = \frac{\sigma\sqrt{6}}{\pi} \quad \& \quad \zeta = \bar{R} - \delta \cdot \beta, \quad (2)$$

153 with  $\sigma$  as the standard **deviation**,  $\bar{R}$  as the mean of the REGNIE sample and  $\delta$  as the Euler-Mascheroni constant ( $\approx .05772$ ).  
154 The return period  $t_{RP}$  is directly related to the probability of occurrence of the threshold  $P(R \geq R_{tr_s}) = t_{RP}^{-1}$  so that the CDF  
155 is given by  $F(R) = 1 - t_{RP}^{-1}$ . The resulting equation to estimate ~~the return period~~  $t_{RP}$  is:

$$156 \quad t_{RP}(R) = \left[ 1 - \exp\left(-\exp\left(\frac{\zeta - R}{\beta}\right)\right) \right]^{-1}. \quad (3)$$

#### 157 **2.1.4 Storm tracks computed from radar reflectivity**

158 Storm motion vectors are computed from three-dimensional (3D) radar reflectivity data from the radar network of DWD.  
159 The data, which includes 17 radar stations with dual-polarization Doppler radars, are combined and interpolated into a radar  
160 composite with a spatial resolution of  $1 \times 1 \text{ km}^2$  (Cartesian grid). The temporal resolution of the individual scans is 15 minutes.  
161 Radar reflectivity is available on 12 equidistant vertical levels **extending from 1 km to 12 km above ground level**. For the  
162 whole period between 2005 and 2018, which is used to relate the storm motions computed for the investigation period to the  
163 climatology (Sect. 4.1), data were stored in six reflectivity classes only. The two highest classes, which are considered here,  
164 range from 46 to 55 dBZ and  $\geq 55$  dBZ.

165 To identify storm tracks, the cell-tracking algorithm TRACE3D (Handwerker, 2002) was adapted to the DWD radar compos-  
166 ite in Cartesian coordinates. Once the algorithm detects a convective cell core, it can be re-detected in consecutive time steps  
167 and merged into an entire cell track. Storms are defined by having a minimum reflectivity core of 55 dBZ (corresponding to the  
168 highest class) and a vertical extent of at least 1 km. Thus, only severe convective storms frequently associated with hazardous  
169 weather are considered. Thunderstorms above the 55 dBZ threshold usually form a well-defined core of high reflectivity that  
170 can be easily and reliably tracked. Based on TRACE3D, information about width, length, duration, and propagation speed, as  
171 well as direction, is available for each individual thunderstorm track. Note that we mainly use tracking to estimate the propaga-  
172 tion speed and direction of the cells (Sect. 3 and Sect. 4.1). Even if weaker cells are not detected using the 55 dBZ thresholds, it  
173 can be assumed (**cf. Video Supplement for two representative days**) that they cannot move **with** higher speeds. More details  
174 about data and the tracking method can be found in Puskeiler et al. (2016) and Schmidberger (2018). Due to a lack of 3D radar  
175 data for the other countries in 2018, our investigation refers only to severe convective storms that occurred in Germany.

#### 176 **2.1.5 Sounding stations**

177 Atmospheric conditions are estimated from vertical profiles of temperature, moisture, wind speed and direction at seven sound-  
178 ing stations provided by DWD and the Integrated Global Radiosonde Archive (IGRA) from the National Climatic Data Center  
179 (Durre et al., 2006). These stations are distributed over the entire domain: Bordeaux ( $44.83^\circ\text{N}$ ,  $0.68^\circ\text{W}$ ) and Trappes ( $48.77^\circ\text{N}$ ,  
180  $2.00^\circ\text{E}$ ) in France; Essen ( $51.41^\circ\text{N}$ ,  $6.97^\circ\text{E}$ ), Stuttgart ( $48.83^\circ\text{N}$ ,  $9.20^\circ\text{E}$ ), and Munich ( $48.24^\circ\text{N}$ ,  $11.55^\circ\text{E}$ ) in Germany; Pay-

181 erne (46.82°N, 6.95°E) in Switzerland, and Vienna (48.23°N, 16.37°E) in Austria (see Fig. 1). Other sounding stations could  
182 not be used because of multiple gaps in the time series.

183 Atmospheric stability can be estimated by indices such as CAPE as well as by the surface-based Lifted Index (SLI; Galway,  
184 1956). The latter, which we use in the following, has proven to be as suitable as CAPE in several studies (e.g. Huntrieser et al.,  
185 1997; Sánchez et al., 2009; Westermayer et al., 2017; Rädler et al., 2018). There are studies, in which SLI has even shown a  
186 better prediction skill than CAPE (e.g. Haklander and van Delden, 2003; Manzato, 2003; Kunz, 2007; Mohr and Kunz, 2013).  
187 In addition to the SLI, we also investigate the horizontal wind speed in 500 hPa (V500). Both variables are analysed at 12 UTC,  
188 several hours ahead of peak thunderstorm activity in central and western Europe (Wapler, 2013; Piper and Kunz, 2017; Enno  
189 et al., 2020).

## 190 2.2 Model data

191 We use the European Centre for Medium-Range Weather Forecasts (ECMWF) high-resolution operational analysis data and  
192 ECMWF ERA-Interim reanalysis (Dee et al., 2011) to describe the large-scale meteorological conditions and calculate weather  
193 regimes (see Sect. 2.3), **perform** kinematic backward trajectories (see Sect. 2.4), and **identify** cut-off lows (see Sect. 2.5).  
194 ECMWF analysis is available 6-hourly interpolated to a regular grid with 0.125° horizontal resolution. ERA-Interim used for  
195 the historical analysis is available 6-hourly interpolated to a regular grid at 1.0° horizontal resolution. Beside the atmospheric  
196 stability (based on SLI), we examine in the study V500, the bulk wind shear (BWS; directional shear) as wind difference  
197 between 10 m and 500 hPa calculated by vector subtraction (e.g. Thompson et al., 2007), 500 hPa geopotential height (Z500)  
198 and the vertically integrated water vapor (IWV).

## 199 2.3 North Atlantic-European weather regimes

200 The large-scale flow conditions in the Atlantic-European region are characterized in terms of a definition of seven year-round  
201 weather regimes based on 10-day low-pass-filtered 500 hPa geopotential height anomalies (Z500<sup>2</sup>; Grams et al., 2017). The  
202 regimes are identified by k-means clustering in the phase-space spanned by the seven leading empirical orthogonal functions  
203 (EOFs). Based on these seven clusters, an active weather regime life-cycle is derived from the normalized projection of each  
204 6-hourly anomaly in the cluster mean following Michel and Rivière (2011). Thereby, time steps with weak projections are  
205 filtered out (no regime). An active regime life-cycle persists for at least 5 days but fulfills further criteria as described in Grams  
206 et al. (2017).

207 Our weather regime definition is in line with ‘classical’ concepts of four seasonal regimes for Europe (e.g. Vautard, 1990;  
208 Michelangeli et al., 1995; Ferranti et al., 2015), but reflects important seasonal differences. Three of the seven regimes are  
209 dominated by a negative **Z500 anomaly** and enhanced cyclonic activity (see Supplementary Fig. 1). These are the *Atlantic*  
210 *Trough (AT)* regime with a trough extending towards western Europe, the *Zonal regime (ZO)* with cyclonic activity around  
211 Iceland, and the *Scandinavian Trough (ScTr)* regime with a trough shifted towards the east. The remaining four regimes are  
212 characterized by a positive **Z500 anomaly** centered at different locations and therefore referred to as ‘blocked regimes’. These  
213 are the *Atlantic Ridge (AR)* regime, with a blocking ridge over the eastern North Atlantic and an accompanying trough extend-

214 ing from eastern Europe into the central Mediterranean, the *European Blocking (EuBL)* regime, with a blocking anticyclone  
215 extending from Western Europe to the North Sea, *Scandinavian Blocking (ScBL)*, with high-latitude blocking over Scandinavia,  
216 and *Greenland Blocking (GL)* with a blocking ridge over the Greenland-Icelandic region.

## 217 **2.4 Lagrangian Analysis Tool**

218 The path of the air masses during the thunderstorm period from 22 May to 12 June is traced by calculating 10-day kine-  
219 matic backward trajectories from ERA-Interim using the Lagrangian Analysis Tool (LAGRANTO, Wernli and Davies, 1997;  
220 Sprenger and Wernli, 2015). The trajectories are initialised every 6 hours on each day of the study period from the **nearest**  
221 **ERA-Interim grid points to the surrounding site and its immediate neighbours to the north, south, east, and west** (Fig. 1  
222 yellow squares). In order to represent the Lagrangian history of moist, low-tropospheric air masses that contributed to the  
223 severe thunderstorms, trajectories are initialised every 50 hPa between 950 and 600 hPa. ~~where the air masses relevant for the~~  
224 ~~thunderstorm development are located.~~

## 225 **2.5 Identification of PV cut-off low and matching with lightning data**

226 We identify upper-level cut-off lows based on PV on the 325 K isentropic surface from ERA-Interim using the algorithm of  
227 Wernli and Sprenger (2007) and Sprenger et al. (2017). The optimal level for the inspection of weather systems on isentropic  
228 surfaces depends on the season. The specific level of 325 K used here is motivated by **previous studies** (cf. R othlisberger et al.,  
229 2018) and the inspection of isentropic PV charts for our case. The algorithm searches for closed areas of PV larger than 2 PVU,  
230 which are disconnected from the main PV reservoir that expands across the North Pole.

231 Following earlier approaches to match weather objects with surface weather (e.g. cyclones and precipitation; Pfahl and  
232 Wernli, 2012a, b), the identified PV cut-off lows (including their PV filaments) are then related to thunderstorm events using  
233 lightning data on the  $10 \times 10 \text{ km}^2$  grid cells. We utilize the smallest distance approach to link a grid cell in the lightning data set  
234 to a grid point in the PV cut-off data set. The different grid sizes between the model and observation data sets require matching  
235 multiple grid cells (lightning data) to one PV cut-off grid point. This means if a grid point shows the presence of a PV cut-off,  
236 all flashes from the associated grid cells are linked to it.

237 To account for the far-field impact of lifting and destabilization by a PV cut-off, we expand the PV cut-off mask by a buffer.  
238 This scale is estimated from the typical Rossby radius of deformation

$$239 \quad L_R = \frac{N \cdot H}{f_0} \quad (4)$$

240 associated with a PV cut-off. Here,  $N$  is the Brunt-V ais al a frequency,  $H$  is the scale height, and  $f_0$  is the Coriolis parameter.  
241 For characteristic values in mid-latitudes with  $N = 0.01 \text{ s}^{-1}$  and  $f_0 = 10^{-4} \text{ s}^{-1}$ ,  $N/f_0$  is typically in the order of 100. A  
242 scale height of 10 km leads to a Rossby deformation radius of 1,000 km, which is typical for synoptic scales. We assume that  
243 some of the PV cut-offs during the study period have a vertical extent of less than 10 km. Therefore, we chose a conservative  
244 deformation radius (buffer) of about 500 km. The robustness of the chosen deformation radius is investigated both qualitatively  
245 and quantitatively. We found that a change in the radius of 100 km, for example, leads to an increase or decrease of around

246 10 % in the total amount of lightning strikes associated with a PV cut-off during our study period (see Supplement Sect. 2).  
247 Such small changes do not affect the qualitative interpretation of our results.

## 248 **2.6 Persistence analysis**

249 Days with constant atmospheric conditions tend to form temporal clusters of certain weather phenomena (here thunderstorms)  
250 lasting of several days (events). This behavior can be described statistically by the concept of persistence. The **event length**  
251 **or duration  $n$  is determined by the number of days, on which a certain criterion is fulfilled (e.g. thunderstorm day or**  
252 **certain atmospheric conditions). Each day is assigned either the value 1 (event day = criterion fulfilled) or 0 (non-event**  
253 **day = criterion not fulfilled). Within a seven-day sequence, we allow one non-event day (skip day, not counted in the**  
254 **total length  $n$ ) without breaking the event. This means that an event lasting up to 7 (14/21) days may contain at most 1**  
255 **skip day (2/3 skip days). For more information on the concept see PIP16.**

256 In the study, we investigate the co-occurrence of low stability (using SLI) and low mid-tropospheric wind speeds (using  
257 V500). For this purpose, the same thresholds as in PIP16 are chosen, which were used to investigate the exceptional atmospheric  
258 conditions of a similar thunderstorm episode. We employ their basic criterion, which is fulfilled if both conditions apply:  
259  $SLI < 0$  K and  $V500 < 10 \text{ m s}^{-1}$  ( $TH_{BC}$ ). In addition, we also discuss our results in context with the strict criterion, which  
260 is fulfilled with  $SLI < -1.3$  K and  $v_{500hPa} < 8 \text{ m s}^{-1}$  ( $TH_{SC}$ ). ~~Both thresholds were originally determined by choosing the~~  
261 ~~maximum of the daily minima in the case study to capture the prevailing (exceptional) atmospheric conditions.~~

## 262 **3 Description of the thunderstorm episode 2018**

263 The period from the first of May to mid-June 2018 was characterized by a large number of thunderstorms that spread across the  
264 study area, several of which were associated with heavy rainfall, hail, and strong wind gusts (see **ESWD reports in** Fig. 2a).  
265 ~~More than 1,500 severe weather reports were collected and archived by the ESWD in our study area during that period.~~  
266 Lightning strikes were recorded on each day, and the affected area ranges between  $100 \text{ km}^2$  on 19 June and  $1,140,000 \text{ km}^2$  on  
267 27 May (accumulations of the  $10 \times 10 \text{ km}^2$  grid cell).

268 The three-week period from 22 May until 12 June was the most active thunderstorm episode in May/June 2018 with a total  
269 of 868 heavy rain, 144 hail, and 145 convective wind gust reports based on the ESWD. The highest number (152 reports)  
270 was issued on 29 May, followed by 31 May (137 reports), most of them reporting heavy rainfall leading to several flash floods  
271 and landslides, which destroyed buildings, vehicles, streets and even railway tracks (DWD, 2018a; WetterOnline, 2018b).  
272 On average, an area of  $758,000 \text{ km}^2$  – twice the size of Germany – was affected by lightning per day, with the result that  
273 thunderstorms covered the entire study area. As shown in Figure 2b, most of the severe weather reports during the episode  
274 came from the western part of France, Benelux, central and southern Germany, and the easternmost part of Austria. While the  
275 spatial distribution of the ESWD reports shows several regional gaps due to an under-representation of eyewitness reports, for  
276 example, in Central and southeastern France (cf. Groenemeijer et al., 2017; Kunz et al., 2020), thunderstorm days are observed

277 throughout the study area (see Supplementary Fig. 4). The extraordinarily large number of thunderstorms, several of them  
278 severe, and the unusual persistence of that situation over three weeks motivated us to select that time frame as the study period.

279 Figure 3 summarizes the evolution of **1-hour** (1 h) and 3-hour (3 h) rain gauge measurements in the study area exceeding  
280 the ESWD heavy rain criteria of 35 mm and 60 mm, respectively. The 1 h criterion was fulfilled during the study period 167  
281 times (Fig. 3a) and an average of about 7.6 stations per day with a variability between one and 20 stations. This highest number  
282 of stations belongs to the day with the second most ESWD severe weather reports (31 May). The 3 h criterion was reached 38  
283 times, with a maximum of at least 5 stations on three days. The location of the respective stations shows heavy rain events in  
284 all of the countries under consideration without any clustering (Fig. 3b,c).

285 During the episode, the thunderstorms developed mainly as isolated cells and clusters of several cells, the latter preferably  
286 in the early evening and night. Only on a few days (e.g. on 22 May or 1 June) larger mesoscale convective systems (MCS)  
287 formed, which persisted during the night and early morning. Animated images of radar reflectivity can be found in the Video  
288 Supplement for two representative days: 27 and 31 May. The two animations show a large number of both isolated thunder-  
289 storms with a short lifetime of approximately 30 min (radar visibility, **i.e. period of precipitation**) and cell clusters persisting  
290 over several hours. Most cells moved very slowly or even remained stationary on the two days.

291 The slow movement of the convective cells, a prominent feature of the entire thunderstorm episode, was mainly due to the  
292 low wind speed at mid-tropospheric levels (cf. Sect. 3.1.2). According to the cell tracking (Germany only; see Sect. 2.1.4),  
293 about half of all cells reaching a radar reflectivity of at least 55 dBZ had a propagation speed of less than  $5 \text{ m s}^{-1}$  (47.3 %  
294 from 480 cells); only a few cells (1.5 %) had a speed above  $15 \text{ m s}^{-1}$  (Fig. 4). Mean, standard deviation, and median values are  
295  $5.9 \text{ m s}^{-1}$ ,  $\pm 2.9 \text{ m s}^{-1}$ , and  $5.2 \text{ m s}^{-1}$ , respectively, which is almost half of the long-term statistics (cf. Sect. 4.1; **see also the**  
296 **propagation speed of some record-breaking 1 h and 3 h rainfall totals in Table 1**). The predominant propagation direction  
297 was from southeast to northwest (26.3 % of the detected cells). However, several cells moved in completely different directions  
298 on the same day – a clear sign that the propagation was not only determined by the (weak) mid-tropospheric wind, but also by  
299 internal dynamic effects induced by cold pools or by pressure disturbances (Markowski and Richardson, 2010; Houston and  
300 Wilhelmson, 2012). Examples of different track directions of neighbouring cells can be seen in the radar animation on 27 May  
301 (14 to 15 UTC, at the coordinates:  $x \sim 250 \text{ km}$  &  $y \sim 600 \text{ km}$ ) or on 31 May (21 to 22 UTC;  $x \sim 400 \text{ km}$  &  $y \sim 700 \text{ km}$ ).

302 A detailed look at the chronological sequence during the episode (Fig. 2b) shows that thunderstorms associated with heavy  
303 rainfall and small hail with diameters of around 2 cm were restricted to Benelux and western Germany on 22 May. Some entries  
304 report flash floods and mudslides, for example in the Heilbronn area (SW Germany). Two days later, on 24 May, the federal  
305 state of Saxony (eastern Germany), the east of Austria, and parts of Belgium were hit by torrential rain accumulations. The  
306 German station Bad Elster-Sohl in Saxony (see Fig. 1) on the border to the Czech Republic, for example, measured a record of  
307  $86.3 \text{ mm}/3 \text{ h}$  and  $154.9 \text{ mm}/24 \text{ h}$ . On 26 May, several wind reports with gust speeds of up to  $29 \text{ m s}^{-1}$  (Poitiers, France; see  
308 Fig. 1) and hail reports indicating hailstones with a diameter of up to 5 cm were recorded in the French coastal region near the  
309 Bay of Biscay.

310 The subsequent time frame from 27 May to 1 June was the most active both in terms of the area affected by lightning and  
311 the number of ESWD reports (Fig. 2a). Widespread thunderstorms were observed mainly in Benelux, Germany, and France,

312 but also sporadically in Switzerland and Austria, many of them associated with large rain accumulations and subsequent  
313 flooding, hail between 2 and 4 cm in diameter, and damaging wind reports. Many of record-breaking 1 h and 3 h rainfall totals  
314 occurred within this period (Table 1). For example, the weather station Bruchweiler (see Fig. 1), located in the west of Germany,  
315 measured a 24 h rain accumulation of 145.0 mm on 27 May (Note that the station only provides reports for the full 24 hours).  
316 However, **the rain fell in a period of 3 hours, with 60 mm falling in just 50 min** (see also Supplementary Fig. 5a). The  
317 corresponding track, derived from TRACE3D, has a **short** length of 21 km and a **low** propagation speed of  $5.7 \text{ m s}^{-1}$  (Table 1).  
318 A second example is on 31 May the exceptionally high 1 h rain accumulation of 85.7 mm measured at Diethenhofen close to  
319 Nuremberg in the south of Germany (see also Fig. 3b), listed high in the ranking of highest 3 h rainfall totals as well. The  
320 station was fully hit by an isolated system, which was relatively stationary. The rain rate above 60 mm was present over 35 min  
321 (see also Supplementary Fig. 5b and Video Supplement).

322 In the first half of June, some hail stones and heavy rainfall were still reported almost daily somewhere in the study domain,  
323 though less frequently than before. Towards the end of the study period, convective activity increased again. Especially on the  
324 last day of the study period, on 12 June, the proportion of gust reports (indicating wind speeds between 25 and  $31 \text{ m s}^{-1}$ ) to  
325 all reports was very large. Thereafter, when environmental conditions became more stable (cf. Sect. 3.1), thunderstorms rarely  
326 occurred. The area affected by lightning decreased considerably and no further severe weather reports were archived in the  
327 ESWD.

328 As we will show later (Sect. 3.1.2), **very low wind shear values prevailed across the study area. In a few cases, deep-**  
329 **layer shear magnitudes were sufficient (BWS up to 20 m/s) for the development of severe storms, with large hail up to**  
330 **5 cm in diameter recorded in Southwest France on 26 and 9 June and in southern Germany on 11 June.** However, these  
331 were exceptional cases.

### 332 3.1 Synoptic overview

333 The synoptic situation prior to the thunderstorm episode in 2018 was embedded in a longer lasting unusual large-scale flow  
334 situation. At the beginning of the extended study period, a large-scale mid-tropospheric area of high geopotential stretched out  
335 from the Azores over central Europe and the Baltic to western Russia (Fig. 5a), attended by a corresponding prolonged lower-  
336 level high-pressure system (not shown). This configuration was associated with the advection of warm and relatively dry air  
337 masses over large parts of Europe. In the second week of May, the pattern transitioned into a blocked situation over Europe (see  
338 Sect. 3.1.1). The geopotential height at 500 hPa depicts the typical *Omega*-like structure with high geopotential over central  
339 Scandinavia, flanked by one pronounced trough upstream over the Northern Atlantic and one downstream over Western Russia  
340 (Fig. 5b). Subsequently, the two troughs turned into enclosed cut-off lows filled with relatively cold air and finally merged  
341 into one system located over central Europe on 15 May (not shown). In the third week of May, the cut-off moved slowly  
342 northeastward on an erratic track while gradually dissipating over central and eastern Europe, leaving a moderately warm and  
343 dry air mass with weak gradients over central Europe (Fig. 5c).

344 The study period from 22 May to 12 June was characterized by a rather stationary and persistent synoptic situation with a  
345 pronounced blocking ridge stretching from Iceland over the North Sea to Scandinavia and Northeast Europe (Fig. 6a). As a

346 consequence of the synoptic setting during this episode, the mid-tropospheric flow was weak over most parts of Europe (see  
347 Sect. 3.1.2). On average, the ridge was flanked by long-wave troughs: one on the western side with the axis pointing from Baffin  
348 Bay to Newfoundland, the other on the eastern side stretching from the Barents Sea to Kazakhstan, while the ridge remained  
349 relatively stationary centered over the North Sea region (Fig. 5c-f).

350 A noticeable feature in the mean 500 hPa geopotential height for this episode is a locally enclosed geopotential minimum  
351 over the Bay of Biscay and its surroundings (Fig. 6a) that emerges from repeating/transient cut-off lows forming on the up-  
352 stream side of the blocking ridge. On 25 May (Fig. 5d), a cut-off low (C1a) approached Iberia – which merged in the next days  
353 with the cut-off located over the Celtic Sea (C1b) – and **contributed to convective initiation** for several storms, first in France  
354 and then in Benelux and Germany (cf. Fig. 2 **and Sect. 3.3**). In the following days, a new cut off (C2; not shown) formed west  
355 of Spain, which subsequently influenced the weather there and disappeared relatively quickly. On 1 June, another cut-off (C3)  
356 advanced from the Atlantic (Fig. 5e), **which, together with C1, contributed to convective activity over France and central**  
357 **Europe (see also ESWD reports on heavy rain in Fig. 5e/f, blue dots). Then, C3 developed into a shallow low-pressure**  
358 **zone in central Europe, where several convergence lines formed.** In addition, this situation provided very moist air (IWV  
359 well above  $30 \text{ kg m}^{-2}$  over large areas) until 9 June in eastern France and central Europe (Fig. 5e,f). In the end phase of the  
360 study period, the next cut-off low (C5) with its associated fronts and convergence lines affected the western half of France and  
361 central and southern Germany and lasted until 12 June (Fig. 5f). Simultaneously, a cut-off (C6) over the British Isles influenced  
362 the weather in northern Europe.

363 The geopotential anomalies at the 500 hPa level, calculated as the deviation from the climatological mean (1981–2010),  
364 exhibit for the study period significant positive values of up to 200 gpm west of Norway (Fig. 6a). In contrast, the area over  
365 southwestern Europe is reflected by negative geopotential anomalies of more than 50 gpm. Qualitatively similar anomaly  
366 patterns are seen in the sea-level pressure distribution (not shown). Simultaneously, the IWV (Fig. 6b) showed distinct positive  
367 anomalies of up to  $9 \text{ kg m}^{-2}$  with a 22-day average of  $24–28 \text{ kg m}^{-2}$ . This finding is in line with the sequential progression  
368 of several cut-off lows approaching southwestern Europe and leading to repeating the advection of warm and moist air masses  
369 towards central and western Europe during the study period.

### 370 3.1.1 North Atlantic-European Weather Regimes

371 In terms of the North Atlantic-European weather regimes, the large-scale flow situation in May was dominated by simultane-  
372 ously active life cycles of a Zonal regime (ZO; dark red in Fig. 7a) and European Blocking (EuBL; green). Climatologically,  
373 the Zonal regime is characterized by a negative 500 hPa geopotential height anomaly centered over southern Greenland and  
374 Iceland, accompanied by a weak positive anomaly over central Europe (cf. Supplementary Fig. 1). The climatological Euro-  
375 pean Blocking regime is characterized by a strong positive geopotential height anomaly over the North Sea region, and a weak  
376 negative anomaly over Baffin Bay.

377 The strong projection in both regimes in May suggests that both the cyclonic anomaly in the Icelandic region and the positive  
378 anticyclonic anomaly over Europe were pronounced but altered in their intensities – as discussed in the previous section. The  
379 alternating dominance of either regime in the first three weeks of May (Fig. 7a) reflects the change of zonal to meridional cir-

380 culation and the persistent blocking situation during our study period. It is striking that enhanced convection and thunderstorm  
381 activity over Europe co-occurred with a weakening of the projection in the Zonal regime (see Section before). Specifically,  
382 the first period of widespread thunderstorms (9–16 May; cf. Fig. 2) coincides with a weakening of zonal conditions and a  
383 dominance of European Blocking from 11 to 18 May. This is interrupted by more zonal conditions from 19 to 21 May, leading  
384 to **a pronounced decrease in convective activity**. The convectively most active period from 26 May to 1 June co-occurs with  
385 a very strong projection into European Blocking and ends when the blocking decays. On 3 June, a transition into the Atlantic  
386 Ridge regime occurs, with blocking shifting into the Northeast Atlantic and western Europe, which coincides with the last  
387 episode of an increased number of convective events from 6 to 12 June.

### 388 3.1.2 Local-scale environmental conditions

389 During the entire May/June period, atmospheric stability was very low over large parts of the study domain as indicated by  
390 sounding data (Fig. 7b). The SLI reached negative values almost every day at 12 UTC at one sounding station at least. During  
391 the first thunderstorm episode from 9 to 16 May with several heavy rain and hail events (cf. Fig. 2), several stations already  
392 show negative SLI values at some days. During the study period, all soundings (with a few exceptions) exhibit permanently  
393 negative SLI values; most of the time the values are far below the basic/strict criterion of PIP16 (cf. Sect. 2.6). For example, the  
394 median of the SLI during the study period was lower than  $-3.0\text{ K}$  for Stuttgart, Munich, Vienna, Trappes, and Payerne. Such  
395 low values represent very conducive conditions for thunderstorm formation (e.g. Haklander and van Delden, 2003; Manzato,  
396 2003; Sánchez et al., 2009; Kunz, 2007; Mohr and Kunz, 2013). In the ECMWF analysis (Fig. 8a), the SLI average over  
397 the study period (12 UTC) was negative for most parts of the domain except for northern Germany, where thunderstorms  
398 occurred infrequently. Furthermore, over large parts of the study domain, the strict criterion was also reached. Due to the  
399 upcoming westerly flow at the end of the study period, instability decreased significantly and SLI returned to positive values  
400 less conducive for deep moist convection (Fig. 7b).

401 Due to the **weak geopotential height gradients** that prevailed during the study period (Fig. 6), horizontal wind speed in  
402 the mid-troposphere was likewise exceptionally low. During the first half of May, 500 hPa wind speed ( $V_{500}$ ) was already  
403 low in the sounding data with values rarely exceeding  $15\text{ m s}^{-1}$  (Fig. 7c), but further dropped significantly at the beginning of  
404 the study period. Averaged over the entire study period, median  $V_{500}$  was  $7\text{ m s}^{-1}$  at the Essen sounding station; at Stuttgart,  
405 Munich, and Vienna values were even lower at around  $5\text{ m s}^{-1}$ . At the other three stations in France and Switzerland, the  
406 median was between  $8$  and  $10\text{ m s}^{-1}$ . The observations are in line with ECMWF analysis, where  $V_{500}$  was between  $5$  and  
407  $10\text{ m s}^{-1}$  on average (particularly low in large parts of Germany and Austria; Fig. 8b).

408 Due to the very low wind speed near the surface,  $V_{500}$  is almost similar to BWS from ECMWF analysis (12 UTC; Fig. 8c).  
409 Mean values of BWS between  $5$  and  $10\text{ m s}^{-1}$  across the study area (except of the Pyrenees region) are a strong indication that  
410 the majority of storms did not developed into highly organized convective systems such as squall lines, MCS or supercells. The  
411 following analyses are relying on  $V_{500}$  instead of BWS, especially because of the very unusually low wind speed at 500 hPa. It  
412 should be noted that the values for the ~~deep-layer shear~~ speed shear are even lower compared to BWS ( $3-9\text{ m s}^{-1}$ ; not shown).

### 413 3.2 Air mass origin and paths during the event

414 The investigation of sounding data revealed an exceptional air mass, which conserved its key properties conducive to convection  
415 in the entire study period. This finding together with the low-pressure gradient associated with the blocking anticyclone over  
416 the European sector (Fig. 6) suggests that the air mass was relatively stationary in western and central Europe during the study  
417 period. To test this hypothesis, 10-day kinematic backward trajectories are calculated to investigate the Lagrangian history  
418 and paths of moist, lower-tropospheric air masses. Though backward trajectories are started from all six sounding stations,  
419 Bordeaux, Stuttgart, and Vienna are chosen as representative locations for the following analysis.

420 The median trajectory pathways during the entire study period 22 May to 12 June consistently show that air masses originated  
421 west of the sounding stations and reached those in a southwesterly flow (Fig. 9a). Already ten days prior to reaching the area of  
422 the sounding stations, two thirds of the air masses were located over the Atlantic-European sector. Though about 50 % of the  
423 air masses were transported over a distance of 5,000 km (Fig. 9b), the median distance from their initial location (i.e. Bordeaux,  
424 Stuttgart, Vienna) never exceeded 2,000 km (Fig. 9c). This clearly indicates that air masses re-circulated while approaching the  
425 area of the sounding stations. Five days prior to arriving at the location, trajectories were mostly located over Europe (bold  
426 ellipses) and within a radius of 1,000 km around the sounding stations.

### 427 3.3 Thunderstorms related to cut-off lows

428 Having shown that a quasi-stationary air mass, which was conducive to convection prevailed over vast parts of central Europe  
429 during the study period, we now explore cut-off low activity **that can prepare the atmosphere for convective initiation  
430 due to the associated large-scale lifting**. The blocking situation over central Europe and the North Sea during the study  
431 period was accompanied by a negative geopotential height anomaly over the Iberian Peninsula (Fig. 6), which corresponds  
432 well with a significantly enhanced frequency of PV cut-offs of more than 50 % in the Bay of Biscay region (Fig. 10a). This  
433 region of enhanced PV cut-off frequencies expands over much of Spain, western France and some parts of the British Isles  
434 with frequencies often above 25 %, but does not reach Germany or eastern Europe. The fact that relatively high PV cut-off  
435 frequencies expand over a larger region of western Europe (Fig. 10a) underlines that multiple individual PV cut-offs form on  
436 the upstream flank of the blocking ridge (see Fig. 5), and intermittently move across Iberia, France, the British Isles, the North  
437 Sea, and Germany.

438 In such a configuration, filaments of positive PV that separate from the main PV cut-off may favour lifting on their down-  
439 stream flank and help to **initiate** deep moist convection over larger areas. This relation is exemplified by a 2-day period from  
440 31 May to 1 June representing the end of the period with the highest lightning activity and number of ESWD reports. Here,  
441 more than 700,000 lightning strikes were measured over the study domain (black bars in Fig. 11) and more than 70 % of these  
442 can be attributed to PV cut-off activity (light grey bars). On 31 May, in the early afternoon, thunderstorms primarily affected  
443 Belgium and the Netherlands first (Fig. 12a), before lightning activity re-emerged over central and northern France, Switzer-  
444 land, and various parts of Germany (Fig. 12b). Several of these events were documented by heavy rain reports in the ESWD  
445 (cf. Fig. 2). During the following night, the slow-moving multicellular system moved from Switzerland northwards affecting

446 the southwestern and the western parts of Germany (Fig. 12c,d; cf. Sect. 3). While the system dissipated in the late morning  
447 over the border region of Germany and Belgium, severe thunderstorms developed again over eastern and northern Germany,  
448 Czech Republic, western Poland, and the Pyrenees (Spain; Fig. 12e,f). The link to upper-level PV filaments becomes apparent  
449 by carefully investigating the 6-hour evolution of the identified cut-off low masks (Fig. 12; cf. Sect. 2.5). Additionally, the area  
450 of negative  $\omega$  values indicates upward vertical motion over larger areas (light blue). Generally, such ascent downstream of a  
451 trough/PV cut-off due to vertically increasing advection of PV in combination with layer thickness advection and destabiliza-  
452 tion underneath the high PV air, which is well represented in our example.

453 On 31 May, a narrow trough approached from the Atlantic to Iberia (cf. Fig. 5e), accompanied by the cut-off low (C3), **which**  
454 **together with C1 forms the identified masks of the PV cut-offs region in Figure 12a. In particular, C1, located above**  
455 **France at that time, and the associated areas of ascent (light blue) correspond well with the regions of thunderstorm**  
456 **activity in southeastern Germany, central France and the Netherlands in the late afternoon (Fig. 12b).** From 12 UTC  
457 until 18 UTC the next day, this trough narrowed while moving gradually northeastward accompanied by enhanced lightning  
458 activity moving from Central France and southern Germany to northeastern Germany and Poland (Fig. 12e,f). It is especially  
459 apparent that the multicellular system, which developed in the evening hours of 31 May (Section 3), emerged in a region of  
460 negative  $\omega$  values ahead of the trough (Fig. 12c). On 1 June ascent occurs further to the east over Austria, the Czech Republic  
461 and northeastern Germany (Fig. 12e), which agrees well with the location of thunderstorm initiation.

462 The above discussion of PV filament evolution and lightning activity from 31 May to 1 June revealed an apparent link of  
463 this feature with lightning activity confined to the downstream side of PV filaments, where lifting is favoured. Considering the  
464 entire study period, we found 54 % of the lightning linked to a nearby PV cut-off (Fig. 11). Examining individual days reveals  
465 that on the day with the highest number of lightning detections (29 May) over 85 % of these events can be linked to a PV  
466 cut-off. Six out of eight days with the highest number of lightning flashes were the days from 27 May to 1 June. During this  
467 period, more than 75 % of the lightning strikes can be connected with one of the PV cut-offs. We conclude that cut-off low  
468 activity provided the necessary environment that favoured lifting within the prevailing unstable air mass and thus **indirectly**  
469 **contributed to convective initiation of** widespread thunderstorms in western and central Europe during this period.

## 470 **4 Historical context**

471 In this section, we assess the exceptional nature of the thunderstorm event, by relating the observed rainfall totals, the prevailing  
472 environmental conditions, and the occurrence of cut-off systems to long-term data records.

### 473 **4.1 Return periods of rainfall and propagation speed of convective cells**

474 To estimate the severity of the rainfalls with respect to the rainfall climatology, we computed return periods (RPs) for each day  
475 during the study period in the REGNIE long-term record based on Equation (3). Afterwards, we determined the highest RP  
476 (largest 24-hour rain total) for each grid point. **This analysis is restricted to Germany due to the availability of long-term**

477 (> 50 years), high-resolution (1 km<sup>2</sup>) gridded rainfall data. REGNIE data derived from measurements at climate stations  
478 certainly underestimate precipitation peaks, but this is the case both for the study period and the 67-years reference period.

479 Extreme precipitation generally occurred locally, and only a few smaller regions were affected by high rainfall totals exceed-  
480 ing RPs of 5 years (Fig. 13). RPs in excess of 10 years were restricted to the southern parts of Germany (south of 52°N), except  
481 for a few grid points south of Berlin. Most of the precipitation fields with higher RPs occurred as clusters; for example, those  
482 near the border to France in Rhineland Palatinate and the Saarland (near Saarbruecken), northeast of Stuttgart, around Bad-  
483 Elster Sohl, or north of Munich. Several local maxima have RPs of up to 50 years, but a few hot spots, unevenly distributed in  
484 southern Germany, reach values in excess of 200 years (e.g. the observation in Bad Elster-Sohl; cf. Sect. 3). ~~For those locations,~~  
485 ~~of course, precipitation was extreme, partly with new all-year records.~~ Several hot spots have an almost circular shape with the  
486 highest value located in the center. **This does not appear to be an artefact of insufficient gauge density, as most events are**  
487 **represented by multiple gauges (not shown). Instead, it likely reflects the very slow propagation of storms.**

488 This characteristic likely reflects the very slow propagation of the thunderstorms, which was substantially lower during the  
489 study period compared to climatology (Fig. 4). Generally, convective storms detected between 2005 and 2017 (May/June: 3,428  
490 cells) show significantly higher values of  $10.2 \pm 4.9 \text{ m s}^{-1}$  (mean  $\pm$  std) and  $9.5 \text{ m s}^{-1}$  (median) compared to  $5.9 \pm 2.9 \text{ m s}^{-1}$   
491 and  $5.2 \text{ m s}^{-1}$  in the study period. Only 14.4 % of all detected cells show values below  $5 \text{ m s}^{-1}$ , which differs significantly from  
492 the proportion in the study period with 47.3%. 15.5 % of the events propagated with a speed of at least  $15 \text{ m s}^{-1}$  (study period  
493 only 1.5%; cf. Sect. 3.1.2).

#### 494 4.2 Environmental conditions

495 We begin the analysis of the environmental conditions by comparing the SLI and V500 values observed at the seven sounding  
496 stations during the study period with comparably low values during a 30-year period. The latter is represented by the annual  
497 minimum of 22-day (same duration as study period) running mean values for May and June during 1981 and 2010. The box-  
498 and-whisker plots (Fig. 14) on the left represent conditions during our study period (all 22 daily values) and on the right the  
499 historical situation (in sum 30 values). **Thus**, each of the 30 values taken into account in the right box-plot of each station has  
500 the same temporal dimension (running mean of a 22-day period) as the median in the left box-plot of each station. **Recall that**  
501 **the low values for both SLI and V500 were the peculiarity during the 2018 thunderstorm episode.**

502 Both for atmospheric stability and mid-tropospheric flow speed, the interquartile range (the middle 50 % of all values) of  
503 the left box-plot is mostly lower than the interquartile range of the right box-plot, illustrating the exceptional environmental  
504 conditions of the 2018 thunderstorm episode. This applies in particular to the stations in Germany and Austria; stations in  
505 France and in Switzerland tend to overlap (slightly) between the two interquartile ranges. As already mentioned in Sect. 3.1.2,  
506 a large portion of SLI and V500 values during the event (left box-plot) are well below the basic and strict thresholds (cf.  
507 Sect. 2.6).

508 To elaborate on both the peculiarity of the co-occurrence of low stability and weak mid-tropospheric flow and its persistence,  
509 we investigate the probability of concurrent events (CE) by following the methodology of PIP16 (see Sect. 2.6) using the same  
510 basic criterion. The **CE duration** for each of the seven sounding stations during the extended study period in 2018 varies

511 between 5 (Trappes) and 28 days (Munich; cf. legend in Fig. 15). At all three German stations, the defined concurrent conditions  
512 prevailed over an extraordinarily long period (Essen: 17 days incl. 3 skip days; Stuttgart: 21 days incl. 1 skip days; Munich 28  
513 days incl. 3 skip days).

514 In order to assess the occurrence probability of **long-duration CEs** event-persistences of CE with long duration, we compare  
515 the **CE duration** for the 2018 thunderstorm episode with a frequency analysis of CE between 1981 and 2017 (May/June;  
516 Fig. 15). In doing so, the different amount of a certain event persistence with the length  $n$  from the past between 1981 and 2017  
517 are determined for each sounding station. Subsequently, the relative frequency of the event persistence  $n$  per station in Figure 15  
518 is determined by dividing the absolute number of event persistence by the total number of all events. For example, the total  
519 number of all events is approximately 100 for Trappes, Bordeaux, and Essen, approximately 150 for Stuttgart and Payerne, and  
520 approximately 200 for Munich and Vienna reflecting the climatological distribution (north-to-south and west-to-east gradient)  
521 of atmospheric stability (Mohr and Kunz, 2013).

522 The exceptional nature of the atmospheric conditions in 2018 is supported by the fact that, for example, the maximum event  
523 persistence of 19 days between 1981 and 2017 (observed in Vienna) was exceeded in 2018 by two of the considered sounding  
524 stations (Stuttgart, Munich). Additionally, when examining the individual stations, it can be seen that the **CE duration** of 2018  
525 at the stations Stuttgart, Essen, Munich and Payerne have never been observed since 1981. The same applies to the Stuttgart  
526 sounding compared with the results in PIP16, where so far a maximum CE event persistence of 16 days (1960–2014, but  
527 summer half-year) has been calculated. Furthermore, the relative frequency of CE at the other stations (Trappes, Bordeaux,  
528 Vienna) is also rare (0.5–2 %).

### 529 **4.3 Cut-off lows**

530 In May and June, cut-off lows particularly affected southern Europe and the Mediterranean region. The highest frequency  
531 during the climatological period from 1981 to 2010 is found over Portugal and Turkey but with values of around 4 % (contour  
532 in Fig. 10b; cf. Nieto et al., 2007b; Wernli and Sprenger, 2007). This means that during a 22-day period (same time horizon of  
533 the study period) in May and June an average of 0.9 days (4 % of 22 days) with PV cut-off can be expected. During the 2018  
534 thunderstorm episode, the anomaly of the PV cut-off frequency from the climatological mean was exceptionally large with  
535 maximum values of around 40 % confined to northern Iberia and the Bay of Biscay in western Europe. This means that in 2018  
536 a PV cut-off was up to 10 times higher than the climatological mean, resulting in 9 additional days. The region of anomalous  
537 PV cut-off activity expands northward over the British Isles and the adjacent Atlantic Ocean and the North Sea, still with an  
538 excess of 20 % (additional 4 days compared to climatological mean). In other regions, PV cut-off occurrence was similar to  
539 the climatological mean. As an orientation, note that the standard deviation of the cut-off low frequency between 1981 to 2010  
540 (May/June) is 3 % over northern Iberia and the Bay of Biscay and between 1 and 2 % over the British Isles (not shown). We  
541 conclude that the unusual blocking situation over Europe effectively caused cut-off formation on its upstream flank, which then  
542 supported a (synoptic) lifting mechanism – the third ingredient for thunderstorm development, together with instability and  
543 available moisture.

545 In this study, we investigated the synoptic characteristics of an unusual three-week period of thunderstorm activity in central  
546 Europe in May/June 2018. Interestingly, atmospheric blocking was key to providing the large-scale setting conducive for  
547 **convection** in its vicinity. Because of the influence of large-scale mechanisms related to the block and affecting the entire  
548 continent, a very high number of thunderstorms affected large parts of western and central Europe during an unusually long  
549 period of three weeks. At the beginning of the thunderstorm period, southwesterly flow induced the advection of warm and  
550 moist air masses into central Europe. Several studies have identified such a flow to provide convection-favouring conditions  
551 (e.g. van Delden, 2001; Kapsch et al., 2012; Mohr, 2013; Merino et al., 2014; Wapler and James, 2015; Nisi et al., 2016; Piper  
552 et al., 2019; Mohr et al., 2019). Subsequently, the low pressure gradient associated with the blocking anticyclone over the  
553 (adjacent) European sector prevented a significant air mass change. Thus, moist and conditionally unstable stratified air masses  
554 were trapped in a stationary flow on the southern flank of high pressure for more than three weeks (and were re-circulated).  
555 A few authors have already identified atmospheric blocking as a relevant influencer for widespread thunderstorms. PIP16, for  
556 example, showed that the exceptional thunderstorm episode in 2016 in Germany was related to the sequence of Scandinavian  
557 and European Blocking. Santos and Belo-Pereira (2019) identified a blocking-like dynamical structure in addition to a Western  
558 European and a Scandinavian trough to be responsible for approximately three-quarters of all hail events across Portugal. By  
559 combining ERA-Interim reanalysis and lightning detections over a 14-years period, Mohr et al. (2019) found that the presence  
560 of a block over the Baltic Sea is frequently associated with increased odds of thunderstorm occurrence due to convection-  
561 favouring conditions on its western flank (southwesterly advection of warm, moist and unstable air masses).

562 Upper-level cut-off lows or filaments of high PV that separate from the main PV cut-off were key in creating conditions  
563 conducive for convective activity on the meso-scale. **Accompanying lifting provides a weak but persistent ascent, which**  
564 **serves to precondition the thermodynamic environment by adiabatic cooling, thereby increasing CAPE and reducing**  
565 **CIN** (Markowski and Richardson, 2010). Or it can generate instability, if an entire column is lifted bodily until complete  
566 saturation in case of potential instability. On several days during the peak thunderstorm activity, we found that the majority of  
567 thunderstorms (based on lightning detections) can be related to a PV cut-off. **Lifting associated with these cut-offs prepared**  
568 **the atmosphere for convective initiation on the downstream flank. Note that the initiation processes themselves are**  
569 **typically associated with phenomena such as convergence lines, orographic lifting, thermally driven circulations, and**  
570 **boundary-layer thermals (Markowski and Richardson, 2010).** The large positive anomaly in PV cut-off frequency, which  
571 seems to be relevant for the exceptionally high number of thunderstorms during the study period, in turn was also related to  
572 atmospheric blocking. The latter repeatedly lead to the elongation of troughs on its upstream flanks, which finally led to several  
573 cut-off lows. The general flow patterns consisting of this spatially extended ridge flanked by troughs persisted over a period of  
574 three weeks.

575 Heavy rain events are a result of continuously high rain rates, whereby the duration of an event is linked to its propagation  
576 speed and the size of the convective system (Doswell et al., 1996). In addition, a high concentration of water vapour at low  
577 levels in the presence of strong updrafts, high environmental relative humidity, significant cloud depth below the freezing level

578 contribute to maximize rain accumulations, and potentially weak vertical wind shear, which tend to be correlated with weak  
579 mid-tropospheric winds (Markowski and Richardson, 2010). Due to the low propagation speeds, which contributes to long  
580 rainfall duration during the thunderstorm episode in 2018, and high rain rates ( $60 \text{ mm h}^{-1}$  continuously over 50 min), some of  
581 the thunderstorms were able to produce torrential amounts of rain locally. Furthermore, the stagnant flow at mid-tropospheric  
582 levels and thus the low vertical wind shear as a consequence of the blocking (cf. PIP16; Mohr et al., 2019) were also conducive  
583 and frequently prevented most thunderstorms from developing into organized systems such as large MCS or supercells (cf.  
584 Weisman and Klemp, 1982; Doswell and Evans, 2003; Markowski and Richardson, 2010). Most of the thunderstorms formed  
585 as short-lived isolated cells or slow-moving multicellular clusters.

## 586 6 Summary and Conclusions

587 In our study, we investigated an exceptionally large number of thunderstorms in western and central Europe over a three-week  
588 period, mid-May to mid-June 2018, using a combination of observational data and model data to gain a more holistic view of  
589 the prevailing dynamical and thermodynamical conditions and the decisive trigger mechanisms for this unusual thunderstorm  
590 episode. Additional data over a climatological period helped to place the event in its historical context. The 2018 thunderstorm  
591 episode was exceptional **in several respects**: (i) the unusual large number of several thousand thunderstorms that caused more  
592 than 5 million lightning strikes (all types) in the study area; (ii) the combination of low stability (negative Lifted Index) and low  
593 wind speed at mid-tropospheric levels ( $\leq 5 \text{ m s}^{-1}$  at some locations) that prevailed almost every day during the 22-day period;  
594 (iii) the large cut-off low frequency **that contributed to convective initiation for the majority of convection development**;  
595 and (iv) the high rainfall totals with several new records (e.g. Dietenhofen  $86 \text{ mm} / 1 \text{ h}$ ) mainly as a consequence of the low  
596 propagation speed of the storms in combination with high rain rates leading to several pluvial flash floods.

597 The other main conclusions drawn from our analyses are:

- 598 – Atmospheric blocking, albeit frequently associated with heatwaves and droughts, provided large-scale environmental  
599 conditions favouring convection in its vicinity when unstably stratified air masses are advected into Europe and/or be-  
600 come entrapped in stagnant flow.
- 601 – In the present paper, blocking is accompanied by a high cut-off frequency on its upstream side, which together with  
602 filaments of high PV provided the meso-scale setting for deep moist convection. Compared to climatology, the number  
603 of cut-off lows in parts of the study area during the study period was up to 10 times higher.
- 604 – The exceptional persistence of low stability combined with weak wind speed in the mid-troposphere prevailing over  
605 more than three weeks in some regions, especially in Germany and Austria, has never been observed during the past  
606 climatological period of 30 years. This situation was similar to the 2016 thunderstorm episode documented by PIP16,  
607 but with a much longer persistence.

608 – Blocking often associated with low mid-tropospheric wind speeds/low wind shear (cf. Mohr et al., 2019) reduces the  
609 development in severe organized convective systems. However, because of the low propagation speed of the storms  
610 related to the low-pressure gradient within the block, torrential rainfalls can occur on a local scale.

611 A growing understanding of the relationship between atmospheric blocking and deep moist convection can enhance – due  
612 to the associated persistence – the forecast horizon of thunderstorms on sub-seasonal time scales beyond the classical weather  
613 forecast time scale of a few days. This may, for example, help with disaster management, large outdoor activities, and the  
614 agriculture sector. It is only helpful, however, if blocked areas are correctly predicted. Recent studies show that this remains  
615 a challenge for present numerical weather prediction and climate models (Ferranti et al., 2015; Grams et al., 2018), which,  
616 for example, underestimate the blocking frequency in the Atlantic-European sector (Quinting and Vitart, 2019; Attinger et al.,  
617 2019).

618 In future, we intend to investigate statistically some of this study’s results, such as the relationship between blocking, cut-  
619 off lows, air mass transport, and thunderstorm probability. Furthermore, we want to distinguish between different hazard  
620 types (hail, heavy rain, gusts) and associated types of thunderstorms and blocking regimes that reveal possible differences in  
621 atmospheric processes(e.g. jet stream).

622 *Acknowledgements.* The authors thank the various national weather service (DWD; MeteoSwiss; Météo-France; Royal Netherlands Me-  
623 teorological Institute, KNMI; Zentralanstalt für Meteorologie und Geodynamik; ZAMG), the European Climate Assessment and Dataset  
624 (ECA&D) project, the Blitz-Informationdienst von Siemens (BLIDS; namely Stephan Thern), the Integrated Global Radiosonde Archive  
625 (IGRA) and the European Severe Storms Laboratory (ESSL) for providing different observational data sets. In addition, we thank the Euro-  
626 pean Centre for Medium-Range Weather Forecasts (ECMWF) for providing the operational analysis and the ERA-Interim reanalysis data.  
627 The data analysis and visualisation was partly done using the NCAR Command Language (UCAR/NCAR/CISL/VETS, 2019). Furthermore,  
628 we thank Michael Sprenger (ETH Zurich) for compiling the ERA-Interim PV cutoff climatology and Florian Ehmele (KIT) for the post-  
629 processing of the REGINE data (return periods). The contributions of CMG, JFQ, and JaWa were funded by the Helmholtz Association  
630 as part of the Young Investigator Group „Sub-Seasonal Predictability: Understanding the Role of Diabatic Outflow“ (SPREADOUT; grant  
631 VH-NG-1243). We acknowledge the constructive comments two anonymous reviewers, which helped to improve the quality of the paper.

632 *Data availability.* REGNIE (doi:10.1127/0941-2948/2013/0436), German precipitation data, and 3D radar data used in this paper are freely  
633 available for research and can be requested at DWD. Tracks of severe convective storms were calculated from the DWD radar data and are  
634 not freely available, but can be made available on request to Michael Kunz for research. Data from ECA&D can be downloaded via the  
635 project website (<https://www.ecad.eu>), from Météo-France via [https://donneespubliques.meteofrance.fr/?fond=rubrique&id\\_rubrique=26](https://donneespubliques.meteofrance.fr/?fond=rubrique&id_rubrique=26),  
636 from MeteoSwiss via <https://www.meteoswiss.admin.ch/home/services-and-publications/beratung-und-service/datenportal-fuer-lehre-und-forschung.html>, and from ZMAG via <https://www.zamg.ac.at/cms/de/klima/produkte-und-services/daten-und-statistiken/messdaten>. Sound-  
637 ing data are available from the Integrated Global Radiosonde Archive ([https://www.ncdc.noaa.gov/data-access/weather-balloon/integrated-  
638 global-radiosonde-archive](https://www.ncdc.noaa.gov/data-access/weather-balloon/integrated-global-radiosonde-archive)) and data from the ESWD can be obtained via <https://www.eswd.eu> (see terms and conditions for academic or  
639

640 commercial use). Lightning data are not freely available, but can be requested from the Blitz-Informationdienst von Siemens (<http://blids.de>).  
641 ECMWF ERA-Interim reanalysis and operational analysis are also online available via <https://apps.ecmwf.int/datasets/data/interim-full-daily>  
642 and the TIGGE webpage (control forecast step 0; <https://apps.ecmwf.int/datasets/data/tigge>). The methods to detect cut-off lows based on  
643 these data are given in Wernli and Sprenger (2007) and Sprenger et al. (2017) and for weather regimes in Grams et al. (2017).

644 *Author contributions.* All KIT authors jointly conceived the research questions of the study, continuously discussed the results and wrote the  
645 text passages for their respective contribution. SM analysed the ESWD data and together with JaWi the environmental conditions during the  
646 thunderstorm episode and in a historical context. In addition, SM wrote the introduction part together with CMG and the discussion/summary  
647 part of the paper together with MK and prepared the final draft version of the paper. JaWi also described the synoptic overview and the rainfall  
648 statistics in 2018, which were produced by HJP. The return periods of rainfall were investigated by MK, who also examined the lightning data.  
649 Based on LAGRANTO, JQ performed backward trajectory analysis. MS contributed with the analyses of the storm track data (propagation  
650 speed of convective cells). RP generated the PV cut-off data and its relationship to lightning activity was analysed by JaWa and CMG. In  
651 addition, CMG contributed with the analysis of the weather regimes. Finally, all co-authors edited the final draft and provided substantial  
652 comments and constructive suggestions for scientific clarification and further improvements.

653 *Competing interests.* The authors declare that they have no conflict of interest.

654 *Supplement.* The supplement related to this article is available online at: <https://doi.org/10.5194/jn-0-1-2020-supplement>.

655 *Video supplement.* Video supplement related to this paper is available from the Repository KITopen at:  
656 <https://doi.org/10.5445/IR/1000118571> and <https://doi.org/10.5445/IR/1000118574>.

657 **References**

- 658 Attinger, R., Keller, J. H., Köhler, M., Riboldi, J., and Grams, C. M.: Representation of atmospheric blocking in the new global non-  
659 hydrostatic weather prediction model ICON, *Meteorol. Z.*, 28, 429–446, <https://doi.org/10.1127/metz/2019/0967>, 2019.
- 660 Barriopedro, D., García-Herrera, R., Lupo, A. R., and Hernández, E.: A climatology of Northern Hemisphere blocking, *J. Climate*, 19,  
661 1042–1063, <https://doi.org/10.1175/JCLI3678.1>, 2006.
- 662 Barthlott, C., Schipper, J. W., Kalthoff, N., Adler, B., Kottmeier, C., Blyth, A., and Mobbs, S.: Model representation of boundary-  
663 layer convergence triggering deep convection over complex terrain: A case study from COPS, *Atmos. Res.*, 95, 172–185,  
664 <https://doi.org/10.1016/j.atmosres.2009.09.010>, 2010.
- 665 Bennett, L. J., Browning, K. A., Blyth, A. M., Parker, D. J., and Clark, P. A.: A review of the initiation of precipitating convection in the  
666 United Kingdom, *Q. J. R. Meteorol. Soc.*, 132, 1001–1020, <https://doi.org/10.1256/qj.05.54>, 2006.
- 667 Bieli, M., Pfahl, S., and Wernli, H.: A Lagrangian investigation of hot and cold temperature extremes in Europe, *Q. J. R. Meteorol. Soc.*, 141,  
668 98–108, <https://doi.org/10.1002/qj.2339>, 2015.
- 669 Bronstert, A., Agarwal, A., Boessenkool, B., Crisologo, I., Fischer, M., Heistermann, M., Köhn-Reich, L., López-Tarazón, J. A., Moran, T.,  
670 Ozturk, U., Reinhardt-Imjela, C., and Wendi, D.: Forensic hydro-meteorological analysis of an extreme flash flood: The 2016-05-29 event  
671 in Braunsbach, SW Germany, *Sci. Total Environ.*, 630, 977–991, <https://doi.org/10.1016/j.scitotenv.2018.02.241>, 2018.
- 672 Browning, K., Blyth, A., Clark, P., Corsmeier, U., Morcrette, C., Agnew, J., Bamber, D., Barthlott, C., Bennett, L., Beswick, K., Bitter,  
673 M., Bozier, K., Brooks, B., Collier, C., Cook, C., Davies, F., Deny, B., Feuerle, T., Forbes, R., Gaffard, C., Gray, M., Rolf Hankers, R.,  
674 Hewison, T., Kalthoff, N., Khodayar, S., Kohler, M., Kottmeier, C., Kraut, S., Kunz, M., Ladd, D., Lenfant, J., Marsham, J., McGregor,  
675 J., Nicol, J., Norton, E., Parker, D., Perry, F., Ramatschi, M., Ricketts, H., Roberts, N., Russell, A., Schulz, H., Slack, E., Vaughan, G.,  
676 Waight, J., Watson, R., Webb, A., and Wieser, A.: The Convective Storms Initiation Project, *Bull. Am. Meteorol. Soc.*, 88, 1939–1955,  
677 <https://doi.org/10.1175/BAMS-88-12-1939>, 2007.
- 678 Corfidi, S. F.: Cold pools and MCS propagation: Forecasting the motion of downwind-developing MCSs, *Weather Forecast.*, 18, 997–1017,  
679 [https://doi.org/10.1175/1520-0434\(2003\)018<0997:CPAMPF>2.0.CO;2](https://doi.org/10.1175/1520-0434(2003)018<0997:CPAMPF>2.0.CO;2), 2003.
- 680 Dee, D. P., Uppala, S. M., Simmons, A. J., Berrisford, P., Poli, P., Kobayashi, S., Andrae, U., Balmaseda, M. A., Balsamo, G., Bauer, P.,  
681 Bechtold, P., Beljaars, A. C. M., Van De Berg, L., Bidlot, J., Bormann, N., Delsol, C., Dragani, R., Fuentes, M., Geer, A. J., Haimberger,  
682 L., Healy, S. B., Hersbach, H., Hólm, E. V., Isaksen, I., Kållberg, P., Köhler, M., Matricardi, M., McNally, A. P., Monge-Sanz, B. M., Mor-  
683 crette, J. J., Park, B. K., Peubey, C., De Rosnay, P., Tavolato, C., Thépaut, J. N., and Vitart, F.: The ERA-Interim reanalysis: Configuration  
684 and performance of the data assimilation system, *Q. J. R. Meteorol. Soc.*, 137, 553–597, <https://doi.org/10.1002/qj.828>, 2011.
- 685 Dennis, E. J. and Kumjian, M. R.: The impact of vertical wind shear on hail growth in simulated supercells, *J. Atmos. Sci.*, 74, 641–663,  
686 <https://doi.org/10.1175/JAS-D-16-0066.1>, 2017.
- 687 Dole, R. M. and Gordon, N. D.: Persistent anomalies of the extratropical Northern Hemisphere wintertime circulation: Geo-  
688 graphical distribution and regional persistence characteristics, *Mon. Weather Rev.*, 111, 1567–1586, [https://doi.org/10.1175/1520-0493\(1983\)111<1567:PAOTEN>2.0.CO;2](https://doi.org/10.1175/1520-0493(1983)111<1567:PAOTEN>2.0.CO;2), 1983.
- 690 Doswell, C. A. and Evans, J. S.: Proximity sounding analysis for derechos and supercells: An assessment of similarities and differences,  
691 *Atmos. Res.*, 67, 117–133, [https://doi.org/10.1016/S0169-8095\(03\)00047-4](https://doi.org/10.1016/S0169-8095(03)00047-4), 2003.
- 692 Doswell, C. A., Brooks, H. E., and Maddox, R. A.: Flash flood forecasting: An ingredients-based methodology, *Weather Forecast.*, 11,  
693 560–581, [https://doi.org/10.1175/1520-0434\(1996\)011<0560:FFFAIB>2.0.CO;2](https://doi.org/10.1175/1520-0434(1996)011<0560:FFFAIB>2.0.CO;2), 1996.

694 Dotzek, N., Groenemeijer, P., Feuerstein, B., and Holzer, A. M.: Overview of ESSL's severe convective storms research using the European  
695 Severe Weather Database ESWD, *Atmos. Res.*, 93, 575–586, <https://doi.org/10.1016/j.atmosres.2008.10.020>, 2009.

696 Drüe, C., Hauf, T., Finke, U., Keyn, S., and Kreyer, O.: Comparison of a SAFIR lightning detection network in northern Germany to the  
697 operational BLIDS network, *J. Geophys. Res. Atmos.*, 112, D18 114, <https://doi.org/10.1029/2006JD007680>, 2007.

698 Durre, I., Vose, R. S., and Wuertz, D. B.: Overview of the integrated global radiosonde archive, *J. Climate*, 1151, 53–68,  
699 <https://doi.org/10.1175/JCLI3594.1>, 2006.

700 DWD: Schadensrückblick des Deutschen Wetterdienstes: Gefährliche Wetterereignisse und Wetterschä-  
701 den in Deutschland 2018, Deutscher Wetterdienst (DWD), Offenbach, Germany. Available from:  
702 [https://www.dwd.de/DE/presse/pressemitteilungen/DE/2018/20181213\\_schadensrueckblick2018\\_news.html](https://www.dwd.de/DE/presse/pressemitteilungen/DE/2018/20181213_schadensrueckblick2018_news.html) (Accessed 6 March 2020),  
703 2018a.

704 DWD: REGNIE: Regionalisierte Niederschläge Verfahrensbeschreibung und Nutzeranleitung, Deutscher Wetterdienst (DWD), Abteilung  
705 Hydrometeorologie, Offenbach, Germany. Available from: <https://www.dwd.de/DE/leistungen/regnie/regnie.html?nn=353366> (Accessed  
706 13 December 2019), 2018b.

707 DWD: RADOLAN/RADVOR: Hoch aufgelöste Niederschlagsanalyse und -vorhersage auf der Basis quantitativer Radar- und Om-  
708 brometerdaten für grenzüberschreitende Fluss-Einzugsgebiete von Deutschland im Echtzeitbetrieb – Beschreibung des Kompositfor-  
709 mats Version 2.5, Tech. rep., Deutscher Wetterdienst (DWD): Abteilung Hydrometeorologie, Offenbach, Germany. Available from:  
710 <https://www.dwd.de/DE/leistungen/radolan/radolan.html> (Accessed 6 March 2020), 2019.

711 Ehmele, F. and Kunz, M.: Flood-related extreme precipitation in Southwestern Germany: Development of a two-dimensional stochastic  
712 precipitation model, *Hydrol. Earth Syst. Sci.*, 23, 1083–1102, <https://doi.org/10.5194/hess-23-1083-2019>, 2019.

713 Enno, S.-E., Sugier, J., Alber, R., and Seltzer, M.: Lightning flash density in Europe based on 10 years of ATDnet data, *Atmos. Res.*, 235,  
714 104 769, <https://doi.org/10.1016/j.atmosres.2019.104769>, 2020.

715 ESSL: ESWD Event reporting criteria, Last revision: May 10, 2014, European Severe Storms Laboratory e.V., Munich, Germany. Available  
716 from: [https://www.eswd.eu/docs/ESWD\\_criteria\\_en.pdf](https://www.eswd.eu/docs/ESWD_criteria_en.pdf) (Accessed 13 December 2019), 2014.

717 Ferranti, L., Corti, S., and Janousek, M.: Flow-dependent verification of the ECMWF ensemble over the Euro-Atlantic sector, *Q. J. R.*  
718 *Meteorol. Soc.*, 141, 916–924, <https://doi.org/10.1002/qj.2411>, 2015.

719 Galway, J. G.: The lifted index as a predictor of latent instability, *Bull. Am. Meteorol. Soc.*, 37, 528–529, [https://doi.org/10.1175/1520-0477-](https://doi.org/10.1175/1520-0477-37.10.528)  
720 [37.10.528](https://doi.org/10.1175/1520-0477-37.10.528), 1956.

721 Grams, C. M., Binder, H., Pfahl, S., Piaget, N., and Wernli, H.: Atmospheric processes triggering the central European floods in June 2013,  
722 *Nat. Hazards Earth Syst. Sci.*, 14, 1691–1702, <https://doi.org/10.5194/nhess-14-1691-2014>, 2014.

723 Grams, C. M., Beerli, R., Pfenninger, S., Staffell, I., and Wernli, H.: Balancing Europe's wind-power output through spatial deployment  
724 informed by weather regimes, *Nat. Clim. Change*, 7, 557–562, <https://doi.org/10.1038/nclimate3338>, 2017.

725 Grams, C. M., Magnusson, L., and Madonna, E.: An atmospheric dynamics perspective on the amplification and propagation of forecast error  
726 in numerical weather prediction models: A case study, *Q. J. R. Meteorol. Soc.*, 144, 2577–2591, <https://doi.org/10.1002/qj.3353>, 2018.

727 Groenemeijer, P., Půčik, T., Holzer, A. M., Antonescu, B., Riemann-Campe, K., Schultz, D. M., Kühne, T., Feuerstein, B., Brooks, H. E.,  
728 Doswell, C. A., Koppert, H.-J., and Sausen, R.: Severe convective storms in Europe: Ten years of research at the European Severe Storms  
729 Laboratory, *Bull. Am. Meteorol. Soc.*, 98, 2641–2651, <https://doi.org/10.1175/BAMS-D-16-0067.1>, 2017.

730 Gumbel, E. J.: *Statistics of Extremes*, Columbia University Press, New York, USA, 1958.

731 Haklander, A. J. and van Delden, A.: Thunderstorm predictors and their forecast skill for the Netherlands, *Atmos. Res.*, 67–68, 273–299,  
732 [https://doi.org/10.1016/S0169-8095\(03\)00056-5](https://doi.org/10.1016/S0169-8095(03)00056-5), 2003.

733 Handwerker, J.: Cell tracking with TRACE3D — A new algorithm, *Atmos. Res.*, 61, 15–34, [https://doi.org/10.1016/S0169-8095\(01\)00100-4](https://doi.org/10.1016/S0169-8095(01)00100-4),  
734 2002.

735 Hoskins, B. J., McIntyre, M. E., and Robertson, A. W.: On the use and significance of isentropic potential vorticity maps, *Q. J. R. Meteorol.*  
736 *Soc.*, 111, 877–946, <https://doi.org/10.1002/qj.49711147002>, 1985.

737 Houston, A. L. and Wilhelmson, R. B.: The impact of airmass boundaries on the propagation of deep convection: A modeling-based study  
738 in a high-CAPE, low-shear environment, *Mon. Weather Rev.*, 140, 167–183, <https://doi.org/doi:10.1175/MWR-D-10-05033.1>, 2012.

739 Huntrieser, H., Schiesser, H. H., Schmid, W., and Waldvogel, A.: Comparison of traditional and newly developed thunderstorm indices for  
740 Switzerland, *Weather Forecast.*, 12, 108–125, [https://doi.org/10.1175/1520-0434\(1997\)012<0108:COTAND>2.0.CO;2](https://doi.org/10.1175/1520-0434(1997)012<0108:COTAND>2.0.CO;2), 1997.

741 Johns, R. H. and Doswell, C. A.: Severe local storms forecasting, *Weather Forecast.*, 7, 588–612, [https://doi.org/10.1175/1520-0434\(1992\)007<0588:SLSF>2.0.CO;2](https://doi.org/10.1175/1520-0434(1992)007<0588:SLSF>2.0.CO;2), 1992.

743 Kapsch, M. L., Kunz, M., Vitolo, R., and Economou, T.: Long-term trends of hail-related weather types in an ensemble of regional climate  
744 models using a Bayesian approach, *J. Geophys. Res.*, 117, D15 107, <https://doi.org/10.1029/2011JD017185>, 2012.

745 Klein Tank, A. M. G., Wijngaard, J. B., Können, G. P., Böhm, R., Demarée, G., Gocheva, A., Mileta, M., Pashiardis, S., Hejkrlik, L.,  
746 Kern-Hansen, C., Heino, R., Bessemoulin, P., Müller-Westermeier, G., Tzanakou, M., Szalai, S., Pálsdóttir, T., Fitzgerald, D., Rubin, S.,  
747 Capaldo, M., Maugeri, M., Leitass, A., Bukantis, A., Aberfeld, R., van Engelen, A. F. V., Forland, E., Miletus, M., Coelho, F., Mares,  
748 C., Razuvaev, V., Nieplova, E., Cegnar, T., Antonio López, J. A., Dahlström, B., Moberg, A., Kirchhofer, W., Ceylan, A., Pachaliuk, O.,  
749 Alexander, L. V., and Petrovic, P.: Daily dataset of 20th-century surface air temperature and precipitation series for the European climate  
750 assessment, *Int. J. Climatol.*, 22, 1441–1453, <https://doi.org/10.1002/joc.773>, 2002.

751 Kunz, M.: The skill of convective parameters and indices to predict isolated and severe thunderstorms, *Nat. Hazards Earth Syst. Sci.*, 7,  
752 327–342, <https://doi.org/10.5194/nhess-7-327-2007>, 2007.

753 Kunz, M., Wandel, J., Fluck, E., Baumstark, S., Mohr, S., and Schemm, S.: Ambient conditions prevailing during hail events in central  
754 Europe, *Nat. Hazards Earth Syst. Sci. Discuss.* (accepted), <https://doi.org/10.5194/nhess-2019-412>, 2020.

755 Lenggenhager, S. and Martius, O.: Atmospheric blocks modulate the odds of heavy precipitation events in Europe, *Clim. Dynam.*, 53,  
756 4155–4171, <https://doi.org/10.1007/s00382-019-04779-0>, 2019.

757 Lenggenhager, S., Croci-Maspoli, M., Brönnimann, S., and Martius, O.: On the dynamical coupling between atmospheric blocks and  
758 heavy precipitation events: A discussion of the southern Alpine flood in October 2000, *Q. J. R. Meteorol. Soc.*, 145, 530–545,  
759 <https://doi.org/10.1002/qj.3449>, 2018.

760 Manzato, A.: A climatology of instability indices derived from Friuli Venezia Giulia soundings, using three different methods, *Atmos. Res.*,  
761 67, 417–454, [https://doi.org/10.1016/S0169-8095\(03\)00058-9](https://doi.org/10.1016/S0169-8095(03)00058-9), 2003.

762 Markowski, P. and Richardson, Y.: *Mesoscale meteorology in midlatitudes*, John Wiley & Sons, Chichester, UK, 2010.

763 Martius, O., Sodemann, H., Joos, H., Pfahl, S., Winschall, A., Croci-Maspoli, M., Graf, M., Madonna, E., Mueller, B., Schemm, S., Sedlacek,  
764 J., Sprenger, M., and Wernli, H.: The role of upper-level dynamics and surface processes for the Pakistan flood of July 2010, *Q. J. R.*  
765 *Meteorol. Soc.*, 139, 1780–1797, <https://doi.org/10.1002/qj.2082>, 2013.

766 Merino, A., Wu, X., Gascón, E., Berthet, C., García-Ortega, E., and Dessens, J.: Hailstorms in southwestern France: Incidence and atmo-  
767 spheric characterization, *Atmos. Res.*, 140–141, 61–75, <https://doi.org/10.1016/j.atmosres.2014.01.015>, 2014.

768 Michel, C. and Rivière, G.: The link between Rossby wave breakings and weather regime transitions, *J. Atmos. Sci.*, 68, 1730–1748,  
769 <https://doi.org/10.1175/2011JAS3635.1>, 2011.

770 Michelangeli, P.-A., Vautard, R., and Legras, B.: Weather regimes: Recurrence and quasi stationarity, *J. Atmos. Sci.*, 52, 1237–1256,  
771 [https://doi.org/10.1175/1520-0469\(1995\)052<1237:WRRMQS>2.0.CO;2](https://doi.org/10.1175/1520-0469(1995)052<1237:WRRMQS>2.0.CO;2), 1995.

772 Mohr, S.: Änderung des Gewitter- und Hagelpotentials im Klimawandel, Ph.D. thesis, *Wiss. Berichte d. Instituts für Meteorologie und Klimaforschung des Karlsruher Instituts für Technologie*, Vol. 58, KIT Scientific Publishing, Karlsruhe, Germany,  
773 <https://doi.org/10.5445/KSP/1000033828>, 2013.

774 Mohr, S. and Kunz, M.: Recent trends and variabilities of convective parameters relevant for hail events in Germany and Europe, *Atmos. Res.*, 123, 211–228, <https://doi.org/10.1016/j.atmosres.2012.05.016>, 2013.

775 Mohr, S., Wandel, J., Lenggenhager, S., and Martius, O.: Relationship between atmospheric blocking and warm season thunderstorms over  
776 western and central Europe, *Q. J. R. Meteorol. Soc.*, 145, 3040–3056, <https://doi.org/10.1002/qj.3603>, 2019.

777 Morcrette, C., Lean, H., Browning, K., Nicol, J., Roberts, N., Clark, P., Russell, A., and Blyth, A.: Combination of mesoscale and synop-  
778 tic mechanisms for triggering an isolated thunderstorm: Observational case study of CSIP IOP 1, *Mon. Weather Rev.*, 135, 3728–3749,  
779 <https://doi.org/10.1175/2007MWR2067.1>, 2007.

780 Munich Re: Natural catastrophe statistics online – the new NatCatSERVICE analysis tool, Munich Re, Munich, Germany. Available from:  
781 <https://www.munichre.com/en/reinsurance/business/non-life/natcatservice/index.html> (Accessed 13 December 2019), 2019.

782 Nachtnebel, H.-P.: New strategies for flood risk management after the catastrophic flood in 2002 in Europe, in: *Third DPRI-IIASA International Symposium on Integrated Disaster Risk Management: Coping with Regional Vulnerability*, Full Conference Proceedings; 3-5 July  
783 2003, Kyoto International Conference Hall, Kyoto, Japan, 2003.

784 Nieto, R., Gimeno, L., Añel, J. A., De la Torre, L., Gallego, D., Barriopedro, D., Gallego, M., Gordillo, A., Redaño, A., and Delgado,  
785 G.: Analysis of the precipitation and cloudiness associated with COLs occurrence in the Iberian Peninsula, *Meteorol. Atmos. Phys.*, 96,  
786 103–119, <https://doi.org/10.1007/s00703-006-0223-6>, 2007a.

787 Nieto, R., Gimeno, L., De la Torre, L., Ribera, P., Barriopedro, D., García-Herrera, R., Serrano, A., Gordillo, A., Redano, A., and Lorente,  
788 J.: Interannual variability of cut-off low systems over the European sector: The role of blocking and the Northern Hemisphere circulation  
789 modes, *Meteorol. Atmos. Phys.*, 96, 85–101, <https://doi.org/10.1007/s00703-006-0222-7>, 2007b.

790 Nieto, R., Sprenger, M., Wernli, H., Trigo, R. M., and Gimeno, L.: Identification and climatology of cut-off lows near the tropopause, *Ann. NY Acad. Sci.*, 1146, 256–290, <https://doi.org/10.1196/annals.1446.016>, 2008.

791 Nisi, L., Martius, O., Hering, A., Kunz, M., and Germann, U.: Spatial and temporal distribution of hailstorms in the Alpine region: A  
792 long-term, high resolution, radar-based analysis, *Q. J. R. Meteorol. Soc.*, 142, 1590–1604, <https://doi.org/10.1002/qj.2771>, 2016.

793 Ozturk, U., Wendi, D., Crisologo, I., Riemer, A., Agarwal, A., Vogel, K., López-Tarazón, J. A., and Korup, O.: Rare flash floods and debris  
794 flows in southern Germany, *Sci. Total Environ.*, 626, 941–952, <https://doi.org/10.1016/j.scitotenv.2018.01.172>, 2018.

795 Pfahl, S. and Wernli, H.: Quantifying the relevance of atmospheric blocking for co-located temperature extremes in the Northern Hemisphere  
796 on (sub-)daily time scales, *Geophys. Res. Lett.*, 39, L12 807, <https://doi.org/10.1029/2012GL052261>, 2012a.

797 Pfahl, S. and Wernli, H.: Quantifying the relevance of cyclones for precipitation extremes, *J. Climate*, 25, 6770–6780,  
798 <https://doi.org/10.1175/JCLI-D-11-00705.1>, 2012b.

799 Piaget, N., Froidevaux, P., Giannakaki, P., Gierth, F., Martius, O., Riemer, M., Wolf, G., and Grams, C. M.: Dynamics of a local  
800 Alpine flooding event in October 2011: Moisture source and large-scale circulation, *Q. J. R. Meteorol. Soc.*, 141, 1922–1937,  
801 <https://doi.org/10.1002/qj.2496>, 2015.

806 Piper, D. and Kunz, M.: Spatiotemporal variability of lightning activity in Europe and the relation to the North Atlantic Oscillation telecon-  
807 nection pattern, *Nat. Hazards Earth Syst. Sci.*, 17, 1319–1336, <https://doi.org/10.5194/nhess-17-1319-2017>, 2017.

808 Piper, D., Kunz, M., Ehmele, F., Mohr, S., Mühr, B., Kron, A., and Daniell, J.: Exceptional sequence of severe thunderstorms and re-  
809 lated flash floods in May and June 2016 in Germany. Part I: Meteorological background, *Nat. Hazards Earth Syst. Sci.*, 16, 2835–2850,  
810 <https://doi.org/10.5194/nhess-16-2835-2016>, 2016.

811 Piper, D. A., Kunz, M., Allen, J. T., and Mohr, S.: Investigation of the temporal variability of thunderstorms in Central and Western Europe  
812 and the relation to large-scale flow and teleconnection patterns, *Q. J. R. Meteorol. Soc.*, 145, 3644–3666, <https://doi.org/10.1002/qj.3647>,  
813 2019.

814 Poelman, D. R., Schulz, W., Diendorfer, G., and Bernardi, M.: The European lightning location system EUCLID – Part 2: Observations, *Nat.*  
815 *Hazards Earth Syst. Sci.*, 16, 607–616, <https://doi.org/10.5194/nhess-16-607-2016>, 2016., 2016.

816 Portmann, R., Crezee, B., Quinting, J., and Wernli, H.: The complex life cycles of two long-lived potential vorticity cut-offs over Europe, *Q.*  
817 *J. R. Meteorol. Soc.*, 144, 701–719, <https://doi.org/10.1002/qj.3239>, 2018.

818 Puskeiler, M., Kunz, M., and Schmidberger, M.: Hail statistics for Germany derived from single-polarization radar data, *Atmos. Res.*, 178–  
819 179, 459–470, <https://doi.org/10.1016/j.atmosres.2016.04.014>, 2016.

820 Quinting, J. F. and Vitart, F.: Representation of synoptic-scale Rossby wave packets and blocking in the S2S Prediction Project Database,  
821 *Geophys. Res. Lett.*, 46, 1070–1078, <https://doi.org/10.1029/2018GL081381>, 2019.

822 Rädler, A. T., Groenemeijer, P., Faust, E., and Sausen, R.: Detecting severe weather trends using an Additive Regressive Convective Hazard  
823 Model (AR-CHaMo), *J. Appl. Meteorol. Climatol.*, 57, 569–587, <https://doi.org/10.1175/JAMC-D-17-0132.1>, 2018.

824 Rasmussen, P. F. and Gautam, N.: Alternative PWM-estimators of the Gumbel distribution, *J. Hydrol.*, 280, 265–271,  
825 [https://doi.org/10.1016/S0022-1694\(03\)00241-5](https://doi.org/10.1016/S0022-1694(03)00241-5), 2003.

826 Rauthe, M., Steiner, H., Riediger, U., A., M., and Gratzki, A.: A Central European precipitation climatology – Part I: Generation and  
827 validation of a high-resolution gridded daily data set (HYRAS), *Meteorol. Z.*, 22, 235–256, <https://doi.org/10.1127/0941-2948/2013/0436>,  
828 2013.

829 Rex, D. F.: Blocking action in the middle troposphere and its effect upon regional climate: I. An aerological study of blocking action, *Tellus*,  
830 2, 196–211, <https://doi.org/10.3402/tellusa.v2i3.8546>, 1950a.

831 Rex, D. F.: Blocking action in the middle troposphere and its effect upon regional climate: II. The climatology of blocking action, *Tellus*, 2,  
832 275–301, <https://doi.org/10.3402/tellusa.v2i4.8603>, 1950b.

833 Roberts, N. M.: The relationship between water vapour imagery and thunderstorms, Joint Centre for Mesoscale Meteorology Internal Report  
834 No. 110, Met Office, Reading, UK, 2000.

835 Röthlisberger, M. and Martius, O.: Quantifying the local effect of Northern Hemisphere atmospheric blocks on the persistence of summer  
836 hot and dry spells, *Geophys. Res. Lett.*, 43, 10 101–10 111, <https://doi.org/10.1029/2019GL083745>, 2019.

837 Röthlisberger, M., Martius, O., and Wernli, H.: Northern Hemisphere Rossby wave initiation events on the extratropical jet – A climatological  
838 analysis, *J. Climate*, 31, 743–760, <https://doi.org/10.1175/JCLI-D-17-0346.1>, 2018.

839 Russell, A., Vaughan, G., and Norton, E. G.: Large-scale potential vorticity anomalies and deep convection, *Q. J. R. Meteorol. Soc.*, 138,  
840 1627–1639, <https://doi.org/10.1002/qj.1875>, 2012.

841 Sánchez, J. L., Marcos, J. L., Dessens, J., López, L., Bustos, C., and García-Ortega, E.: Assessing sounding-derived parameters as storm  
842 predictors in different latitudes, *Atmos. Res.*, 93, 446–456, <https://doi.org/10.1016/j.atmosres.2008.11.006>, 2009.

843 Santos, J. A. and Belo-Pereira, M.: A comprehensive analysis of hail events in Portugal: Climatology and consistency with atmospheric  
844 circulation, *Int. J. Climatol.*, 39, 188–205, <https://doi.org/10.1002/joc.5794>, 2019.

845 Schaller, N., Sillmann, J., Anstey, J., Fischer, E. M., Grams, C. M., and Russo, S.: Influence of blocking on Northern European and Western  
846 Russian heatwaves in large climate model ensembles, *Environ. Res. Lett.*, 13, 054 015, <https://doi.org/10.1088/1748-9326/aaba55>, 2018.

847 Schmidberger, M.: Hagelgefährdung und Hagelrisiko in Deutschland basierend auf einer Kombination von Radardaten und Versicherungs-  
848 daten, Ph.D. thesis, *Wiss. Berichte d. Instituts für Meteorologie und Klimaforschung des Karlsruher Instituts für Technologie*, Vol. 78,  
849 KIT Scientific Publishing, Karlsruhe, Germany, <https://doi.org/10.5445/KSP/1000086012>, 2018.

850 Schulz, W., Diendorfer, G., Pedebay, S., and Poelman, D. R.: The European lightning location system EUCLID – Part 1: Performance  
851 analysis and validation, *Nat. Hazards Earth Syst. Sci.*, 16, 595–605, <https://doi.org/10.5194/nhess-16-595-2016>, 2016.

852 Sivapalan, M. and Blöschl, G.: Transformation of point rainfall to areal rainfall: Intensity-duration-frequency curves, *J. Hydrol.*, 204, 150–  
853 167, [https://doi.org/10.1016/S0022-1694\(03\)00241-5](https://doi.org/10.1016/S0022-1694(03)00241-5), 1998.

854 Sousa, P. M., Trigo, R. M., Barriopedro, D., Soares, P. M. M., Ramos, A. M., and Liberato, M. L. R.: Responses of European precipita-  
855 tion distributions and regimes to different blocking locations, *Clim. Dynam.*, 48, 1141–1160, <https://doi.org/10.1007/s00382-016-3132-5>,  
856 2017.

857 Sprenger, M. and Wernli, H.: The LAGRANTO Lagrangian analysis tool–version 2.0, *Geosci. Model Dev.*, 8, 2569–2586,  
858 <https://doi.org/10.5194/gmd-8-2569-2015>, 2015.

859 Sprenger, M., Frangkoulidis, G., Binder, H., Croci-Maspoli, M., Graf, P., Grams, C. M., Knippertz, P., Madonna, E., Schemm, S., Škerlak,  
860 B., and Wernli, H.: Global climatologies of Eulerian and Lagrangian flow features based on ERA-Interim, *Bull. Am. Meteorol. Soc.*, 98,  
861 1739–1748, <https://doi.org/10.1175/BAMS-D-15-00299.1>, 2017.

862 Tarabukina, L. D., Antokhina, O. Y., Kononova, N. K., Kozlov, V. I., and Innokentiev, D. E.: Formation of intense thunderstorms in  
863 Yakutia in periods of frequent atmospheric blocking in Western Siberia, in: *IOP Conf. Ser.: Mater. Sci. Eng.*, vol. 698, p. 044050,  
864 <https://doi.org/10.1088/1757-899x/698/4/044050>, 2019.

865 Thompson, R. L., Mead, C. M., and Edwards, R.: Effective storm-relative helicity and bulk shear in supercell thunderstorm environments,  
866 *Weather Forecast.*, 22, 102–115, <https://doi.org/10.1175/WAF969.1>, 2007.

867 Tibaldi, S. and Molteni, F.: On the operational predictability of blocking, *Tellus A*, 42, 343–365, <https://doi.org/10.1034/j.1600->  
868 0870.1990.t01-2-00003.x, 1990.

869 Trapp, R. J.: *Mesoscale-convective processes in the atmosphere*, Cambridge University Press, New York, USA, 2013.

870 UCAR/NCAR/CISL/VETS: The NCAR Command Language (Version 6.6.2) [Software], Boulder, Colorado, USA,  
871 <https://doi.org/10.5065/D6WD3XH5>, 2019.

872 van Delden, A.: The synoptic setting of thunderstorms in Western Europe, *Atmos. Res.*, 56, 89–110, <https://doi.org/10.1016/S0169->  
873 8095(00)00092-2, 2001.

874 van den Besselaar, E. J. M., Klein Tank, A. M. G., and Buishand, T. A.: Trends in European precipitation extremes over 1951–2010, *Int. J.*  
875 *Climatol.*, 33, 2682–2689, <https://doi.org/10.1002/joc.3619>, 2013.

876 Vautard, R.: Multiple weather regimes over the North Atlantic: Analysis of precursors and successors, *Mon. Weather Rev.*, 118, 2056–2081,  
877 [https://doi.org/10.1175/1520-0493\(1990\)118<2056:MWROTN>2.0.CO;2](https://doi.org/10.1175/1520-0493(1990)118<2056:MWROTN>2.0.CO;2), 1990.

878 Wapler, K.: High-resolution climatology of lightning characteristics within Central Europe, *Meteorol. Atmos. Phys.*, 122, 175–184,  
879 <https://doi.org/10.1007/s00703-013-0285-1>, 2013.

880 Wapler, K. and James, P.: Thunderstorm occurrence and characteristics in Central Europe under different synoptic conditions, *Atmos. Res.*,  
881 158, 231–244, <https://doi.org/10.1016/j.atmosres.2014.07.011>, 2015.

882 Weisman, M. L. and Klemp, J. B.: The dependence of numerically simulated convective storms on vertical wind shear and buoyancy, *Mon.*  
883 *Weather Rev.*, 110, 504–520, [https://doi.org/10.1175/1520-0493\(1982\)110<0504:TDonSC>2.0.CO;2](https://doi.org/10.1175/1520-0493(1982)110<0504:TDonSC>2.0.CO;2), 1982.

884 Wernli, H. and Davies, H. C.: A Lagrangian-based analysis of extratropical cyclones. I: The method and some applications, *Q. J. R. Meteorol.*  
885 *Soc.*, 123, 467–489, <https://doi.org/10.1002/qj.49712353811>, 1997.

886 Wernli, H. and Sprenger, M.: Identification and ERA-15 climatology of potential vorticity streamers and cutoffs near the extratropical  
887 tropopause, *J. Atmos. Sci.*, 64, 1569–1586, <https://doi.org/10.1175/JAS3912.1>, 2007.

888 Westermayer, A. T., Groenemeijer, P., Pistotnik, G., Sausen, R., and Faust, E.: Identification of favorable environments for thunderstorms in  
889 reanalysis data, *Meteorol. Z.*, 26, 59–70, <https://doi.org/10.1127/metz/2016/0754>, 2017.

890 WetterOnline: Tornado wütet bei Viersen: Dutzende Häuser stark beschädigt (17.05.2018), WetterOnline Meteorologische Dienstleistungen  
891 GmbH, Bonn, Germany. Available from: [https://www.wetteronline.de/extremwetter/tornado-wuetet-bei-viersen-dutzende-haeuser-stark-](https://www.wetteronline.de/extremwetter/tornado-wuetet-bei-viersen-dutzende-haeuser-stark-beschaedigt-2018-05-17-tv)  
892 [beschaedigt-2018-05-17-tv](https://www.wetteronline.de/extremwetter/tornado-wuetet-bei-viersen-dutzende-haeuser-stark-beschaedigt-2018-05-17-tv) (Accessed 13 March 2020), 2018a.

893 WetterOnline: Unwetterserie Ende Mai: Ganze Ortschaften verwüstet, WetterOnline Meteorologische Dienstleistungen GmbH, Bonn,  
894 Germany. Available from: [https://www.wetteronline.de/extremwetter/unwetterserie-ende-mai-ganze-ortschaften-verwuestet-2018-05-31-](https://www.wetteronline.de/extremwetter/unwetterserie-ende-mai-ganze-ortschaften-verwuestet-2018-05-31-us)  
895 [us](https://www.wetteronline.de/extremwetter/unwetterserie-ende-mai-ganze-ortschaften-verwuestet-2018-05-31-us) (Accessed 13 March 2020), 2018b.

896 WetterOnline: Unwetterserie im Juni: Überflutungen und Hagelmassen (14.06.2018), WetterOnline Meteorologische Dienstleistun-  
897 gen GmbH, Bonn, Germany. Available from: [https://www.wetteronline.de/extremwetter/unwetterserie-im-juni-ueberflutungen-und-](https://www.wetteronline.de/extremwetter/unwetterserie-im-juni-ueberflutungen-und-hagelmassen-2018-06-14-js)  
898 [hagelmassen-2018-06-14-js](https://www.wetteronline.de/extremwetter/unwetterserie-im-juni-ueberflutungen-und-hagelmassen-2018-06-14-js) (Accessed 13 March 2020), 2018c.

899 Wilks, D. S.: *Statistical methods in the atmospheric sciences: An introduction – Second Edition*, Academic Press, Elsevier, Burlington, USA,  
900 2006.

901 Wilson, J. W. and Schreiber, W. E.: Initiation of convective storms at radar-observed boundary-layer convergence lines, *Mon. Weather Rev.*,  
902 114, 2516–2536, [https://doi.org/10.1175/1520-0493\(1986\)114<2516:IOCSAR>2.0.CO;2](https://doi.org/10.1175/1520-0493(1986)114<2516:IOCSAR>2.0.CO;2), 1986.

903 Woollings, T., Barriopedro, D., Methven, J., Son, S.-W., Martius, O., Harvey, B., Sillmann, J., Lupo, A. R., and Seneviratne, S.: Blocking  
904 and its response to climate change, *Curr. Clim. Change Rep.*, 4, 287–300, <https://doi.org/10.1007/s40641-018-0108-z>, 2018.

905 Wussow, G.: Untere Grenzwerte dichter Regenfälle, *Meteorol. Z.*, 39, 173–178, 1922.

**Table 1.** Top list of 1 h, 3 h, and 24 h rainfall totals (in UTC) within the study domain during the study period (AT = Austria, FR = France, GE = Germany). Note that 24 h value means precipitation between 00 and 00 UTC on the next day. Note that some stations only provide reports for the full 24 hours (e.g. Bruchweiler; Mauth-Finsterau). Further analyses regarding rain duration (RD), track length (in km), and propagation speed (in  $\text{m s}^{-1}$ ) and total track area (in  $\text{km}^2$ ) are limited to Germany due to data availability. RD3 means a rain duration with a rain rate  $> 3 \text{ mm h}^{-1}$ , RD35  $> 35 \text{ mm h}^{-1}$ , and RD60  $> 60 \text{ mm h}^{-1}$ . Note two tracks for the German events could not be identified by TRACE3D due to the overlapping of several cells, which were relatively quasi-stationary.

Period	Location (Country)	Coordinates	Rainfall	Time	RD3	RD35	RD60	Length	Speed
1 h	Dietenhofen (GE)	49.4°N, 10.7°E	85.7 mm	31 May 19 h	1 h	45 min	35 min		
1 h	Rohr-Dechendorf (GE)	49.3°N, 10.9°E	71.0 mm	09 June 15 h	1 h	40 min	15 min	84	15
1 h	Labécède-Lauragais (FR)	43.4°N, 2.0°E	64.4 mm	10 June 17 h					
1 h	Hohenberg an der Eger (GE)	50.1°N, 12.2°E	61.4 mm	31 May 18 h	1 h	55 min	30 min	30	6.6
1 h	Lenzkirch-Ruhbühl (GE)	47.9°N, 8.2°E	59.8 mm	31 May 20 h	40 min	30 min	20 min		
1 h	Langres (FR)	47.8°N, 5.3°E	59.4 mm	05 June 20 h					
1 h	Castanet-le-Haut (FR)	43.7°N, 3.0°E	56.2 mm	30 May 14 h					
1 h	Erlbach-Eubabrunn (GE)	50.3°N, 12.4°E	55.6 mm	31 May 17 h	1 h	50 min	35 min	25	4.4
1 h	Rouvroy-en-Santerre (FR)	49.8°N, 2.7°E	54.3 mm	28 May 22 h					
3 h	Prades-le-Lez (FR)	43.7°N, 3.9°E	86.8 mm	11 June 15 h					
3 h	Bad Elster-Sohl (GE)	50.3°N, 12.3°E	86.3 mm	24 May 15 h	3 h	25 min	0 min	16.5	4.6
3 h	Puchberg am Schneeberg (AT)	47.8°N, 15.9°E	86.3 mm	12 June 15 h					
3 h	Dietenhofen (GE)	49.4°N, 10.7°E	86.2 mm	31 May 21 h	~ 1 h 25 min	45 min	35 min		
3 h	L'Oudon-Lieury (FR)	49.0°N, 0.0°E	83.8 mm	28 May 15 h					
3 h	Rocroi (FR)	49.9°N, 4.5°E	79.4 mm	27 May 21 h					
3 h	Leutkirch-Herlazhofen (GE)	47.8°N, 10.0°E	79.1 mm	08 June 18 h	~ 2 h 30 min	45 min	20 min	8.7	3.2
3 h	Kleve (GE)	51.8°N, 6.1°E	78.8 mm	29 May 18 h	~ 2 h 45 min	40 min	20 min	14.5	5.4
3 h	Sulzberg (AT)	47.5°N, 9.9°E	78.0 mm	04 June 18 h					
24 h	Mauth-Finsterau (GE)	48.9°N, 13.6°E	166.5 mm	12 June	~ 8 h 0 min	55 min	20 min	9.2	3.4
24 h	Bad Elster-Sohl (GE)	50.3°N, 12.3°E	154.9 mm	24 May	~ 8 h 15 min	20 min	0 min	16.5	4.6
24 h	Bruchweiler (GE)	49.8°N, 7.2°E	145.0 mm	27 May	~ 2 h 30 min	1 h 5 min	50 min	20.5	5.7
24 h	Monein (FR)	43.3°N, 0.5°W	130.0 mm	12 June					
24 h	Ger (FR)	43.2°N, 0.1°W	126.4 mm	12 June					
24 h	Mont Aigoual (FR)	44.1°N, 3.6°E	124.1 mm	28 May					
24 h	Les Botherreaux (FR)	48.9°N, 0.7°E	123.0 mm	04 June					
24 h	Navarrenx (FR)	43.3°N, 0.8°W	117.0 mm	12 June					
24 h	Puchberg am Schneeberg (AT)	47.8°N, 15.9°E	116.3 mm	12 June					

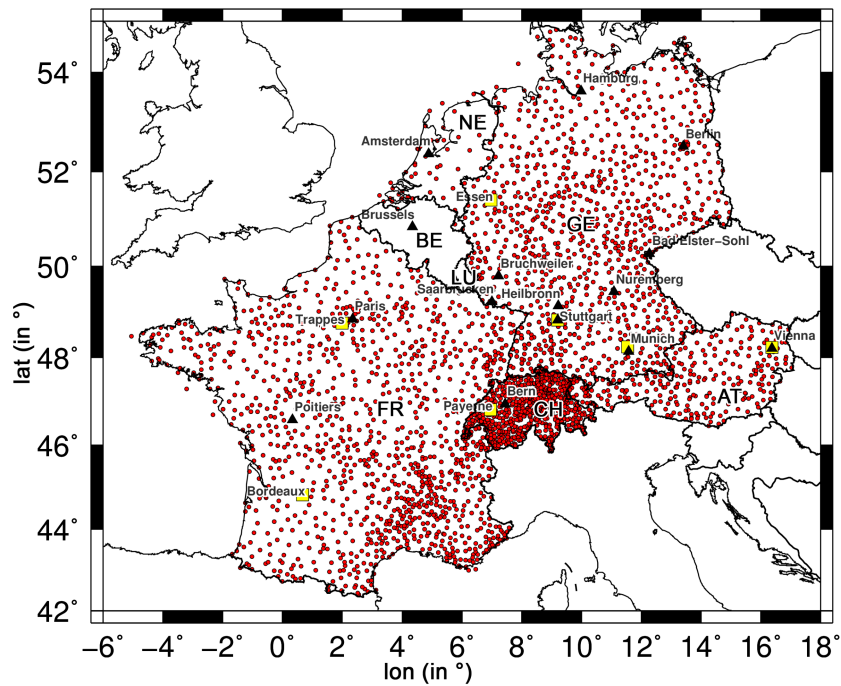


**Figure 1.** All considered precipitation stations (in red) collected from ECA&D and the three national weather services (France, Germany, Switzerland; see Sect. 2.1.3). In addition, the seven investigated sounding stations are shown (in yellow, see Sect. 2.1.5). Some relevant locations are also presented, which are used in the text. Defined country codes are FR = France, BE = Belgium, NE = Netherlands, LU = Luxembourg (the latter three: Benelux), GE = Germany, CH = Switzerland, AT = Austria.

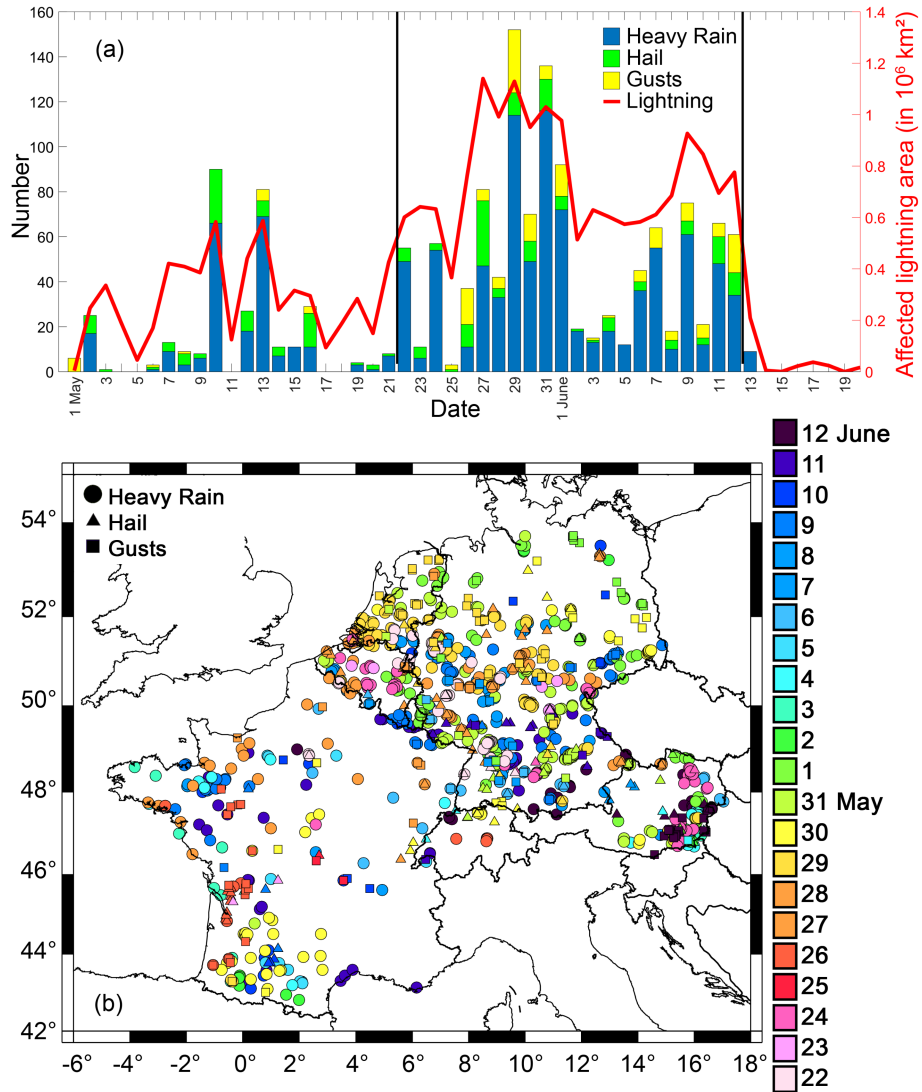


**Figure 2.** (a) Time series of all recorded ESWD reports (heavy rain in blue, hail in green, convective gusts in yellow) in the study domain during the extended study period (i.e. 1 May to 20 June) including the daily total area affected by lightning in km<sup>2</sup> (in red). Vertical black lines indicate the study period (22 May to 12 June 2018). (b) Related regional distribution of the different phenomena (heavy rain ●, hail ▲, convective gusts ■) during the study period.

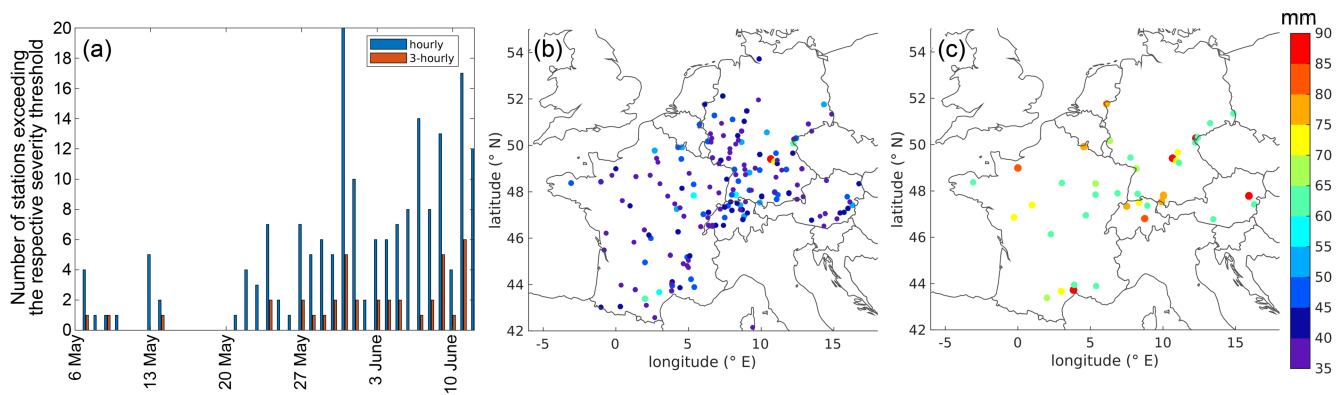


**Figure 3.** (a) Time series of the number of stations exceeding precipitation thresholds of  $> 35$  mm **1-hour** (blue) and  $> 60$  mm over 3-hours (red) including the location and the maximum of (b) **1-hour** and (c) 3-hour **accumulation** of the respective station during the study period (22 May to 12 June).

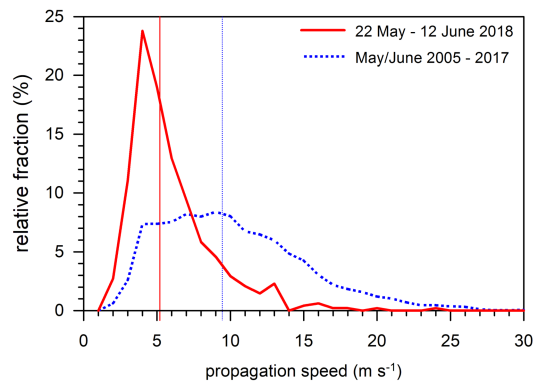


**Figure 4.** Histogram of the propagation speed of convective cells (increments of  $1 \text{ m s}^{-1}$  spline-filter) detected by TRACE3D in Germany during the study period (red) and for all convective cells between 2005 and 2017 (May/June; blue); vertical lines indicate the median of the two samples.

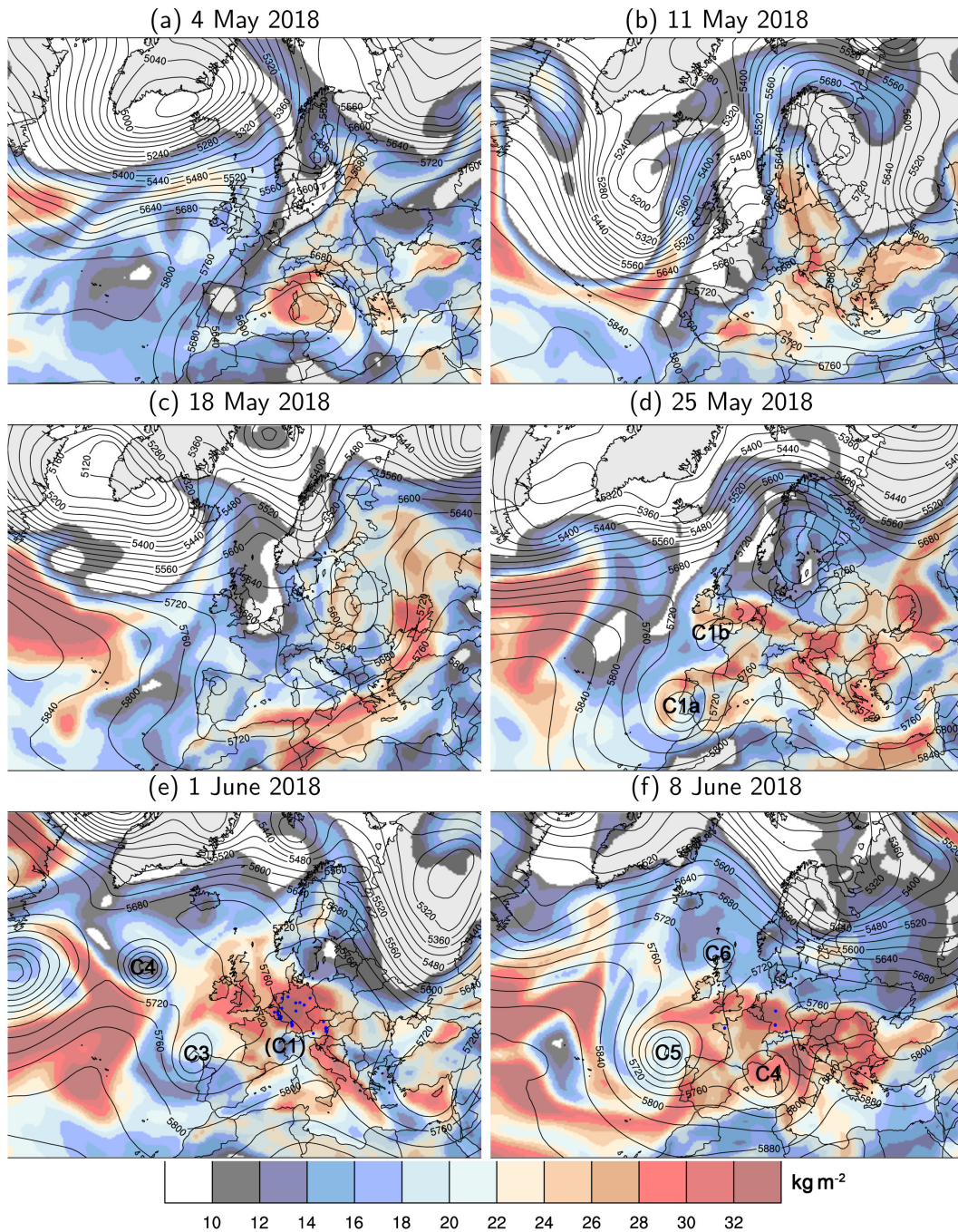


**Figure 5.** 500 hPa geopotential height (contours every 40 gpm) and vertically integrated water vapor (IWV, shaded in  $\text{kg m}^{-2}$ ) for selected days at 00 UTC during the extended study period: (a) 4 May, (b) 11 May, (c) 18 May, (d) 25 May, (e) 1 June, and (f) 8 June (ERA-Interim). Several cut-off lows during the study period mentioned in the text are indicated with numbers (C1, . . . , C6). Small blue dots (in e and f) mark the ESWD reports on heavy rain from Fig. 2. Note that there are no ESWD reports for the first four panels.

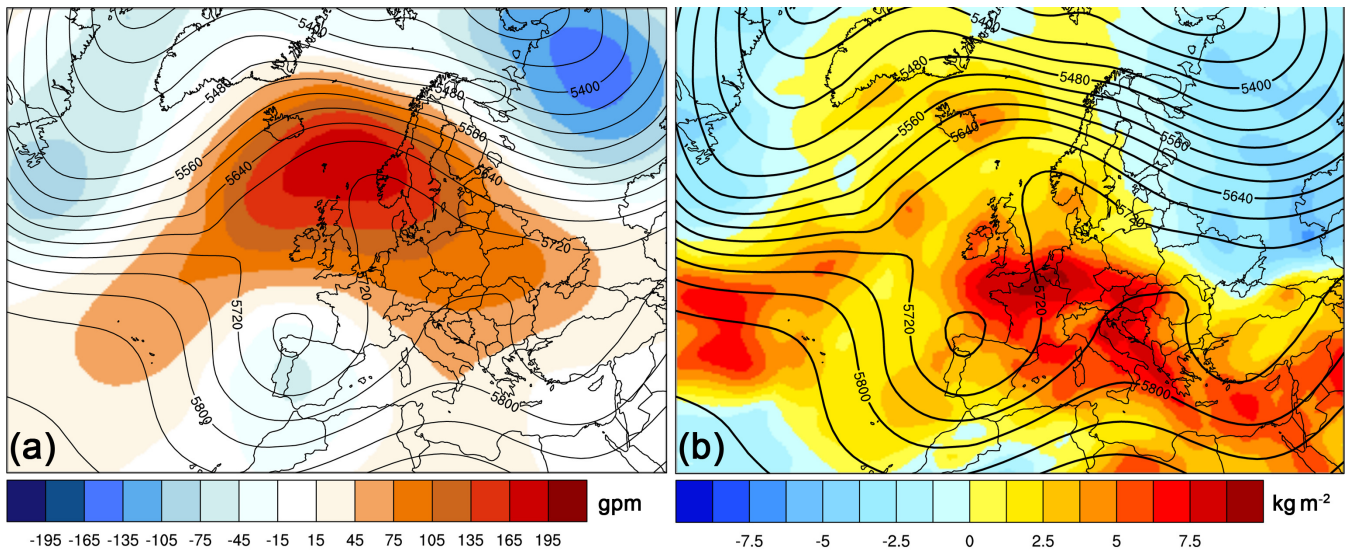


**Figure 6.** Mean anomalies during May/June 2018 of (a) 500 hPa geopotential height anomaly (shaded in gpm) and (b) integrated water vapour anomaly (IWV; shaded in  $\text{kg m}^{-2}$ ), together with the mean 500 hPa geopotential height (contours every 40 gpm). Anomalies are computed with respect to the climatology (1981 – 2001; based on ERA-Interim).

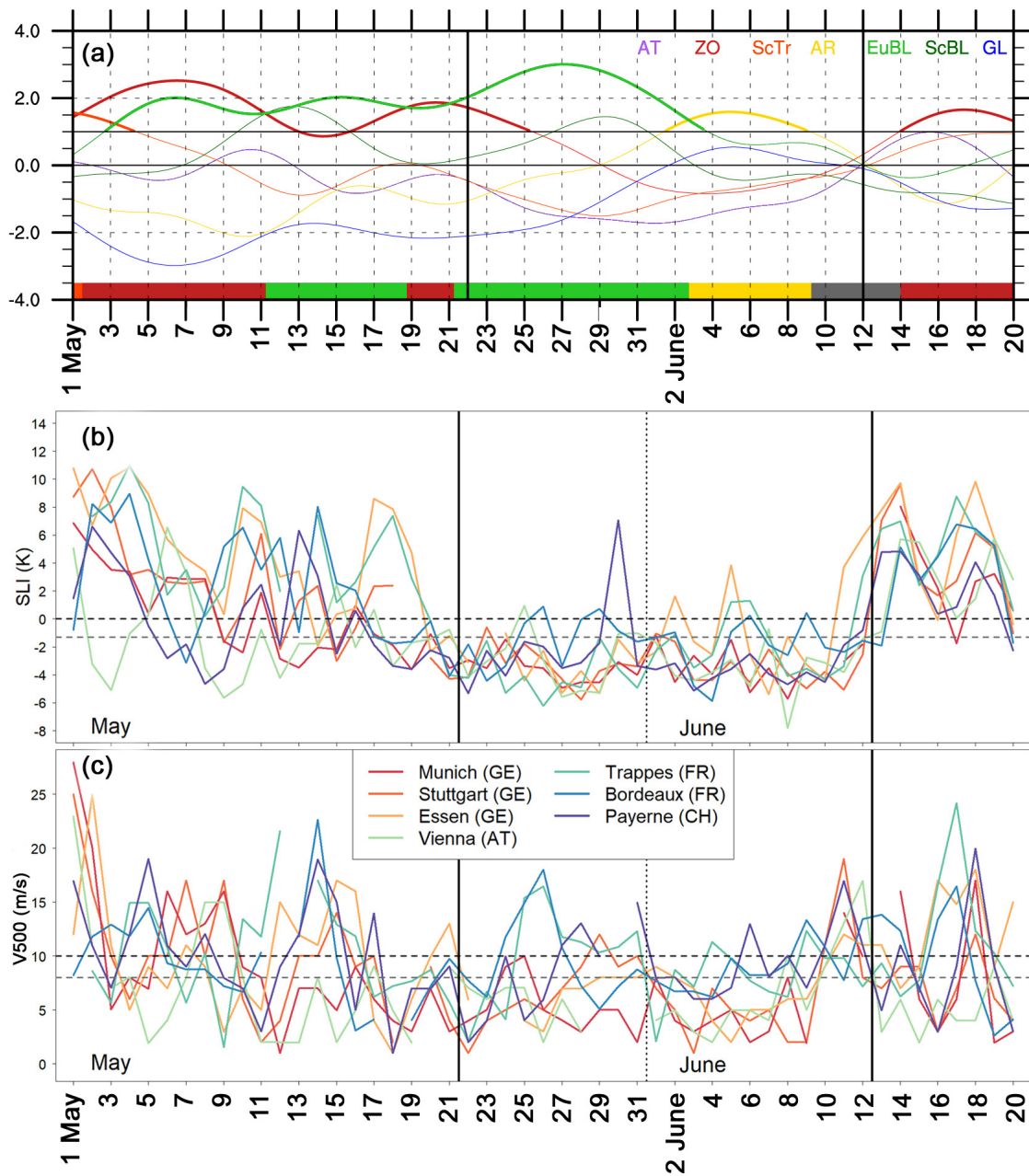


**Figure 7.** Time series of three different parameters during the extended study period from 1 May to 20 June 2018: (a) Atlantic-European weather regime life cycles based on the normalized projection into all seven regimes (colored curves, based on ECMWF analysis). Active regime life cycles with a projection  $> 1.0$  and persistence of at least 5 days are highlighted in bold curves (cf. Sect. 2.3), the dominant regime (maximum projection and active life cycle) is marked at the bottom. Relevant active regime life cycles are: Zonal regime (ZO, dark red), European Blocking (EuBL, light green), Atlantic Ridge (AR, yellow), no regime (grey). (b) Surface-based Lifted Index (SLI in K) and (c) horizontal wind speed at 500 hPa ( $V500$  in  $\text{m s}^{-1}$ ) for the 12 UTC sounding at seven European stations. Horizontal black/gray dashed lines indicate thresholds as defined in PIP16 (Basic criterion:  $0 \text{ K} \ \& \ 10 \text{ m s}^{-1}$ ; Strict criterion:  $-1.3 \text{ K} \ \& \ 8 \text{ m s}^{-1}$ ; cf. Sect. 2.6). Vertical black lines indicate the study period.

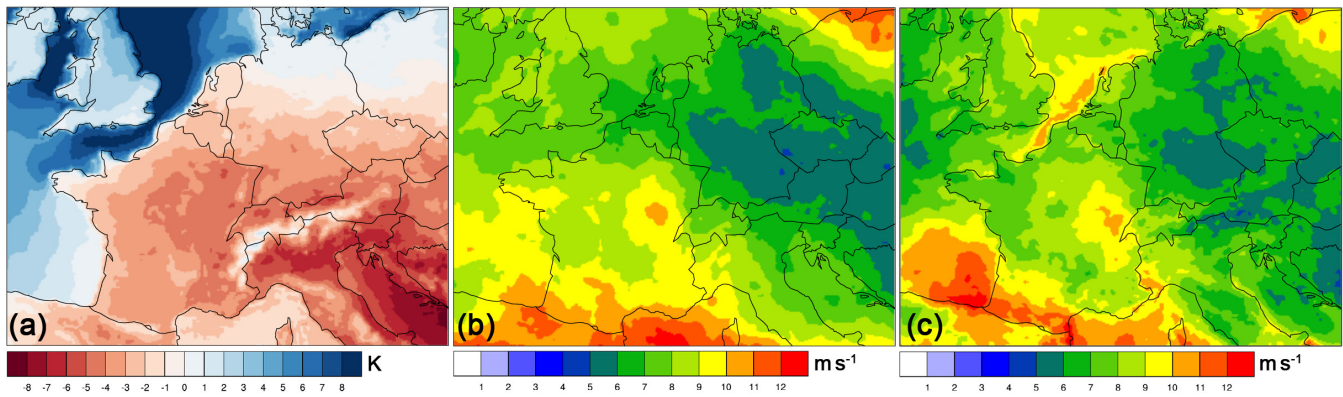


**Figure 8.** (a) Surface-based Lifted Index (SLI in K), (b) horizontal wind speed at 500 hPa ( $V_{500}$  in  $\text{m s}^{-1}$ ), and (c) bulk wind shear between 500 hPa and 10 m (BWS in  $\text{m s}^{-1}$ ) at 12 UTC averaged over the study period from 22 May to 12 June 2018 (ECMWF analysis).

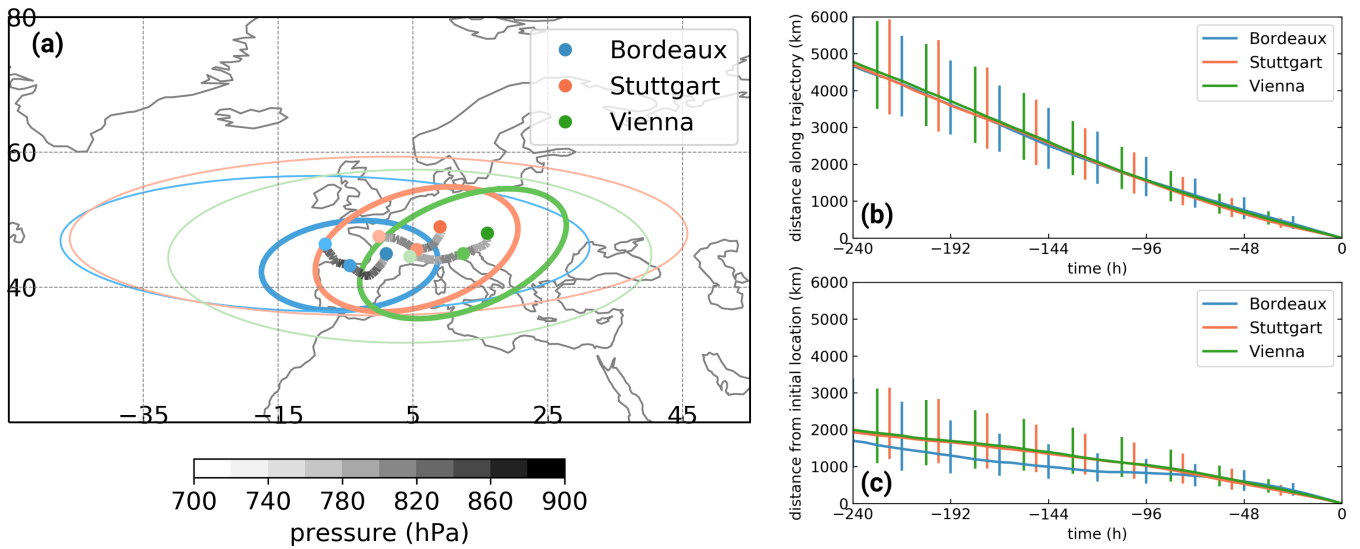


**Figure 9.** 10-day backward trajectory analysis from 22 May to 12 June 2018. (a) Median backward trajectories coloured by their median pressure (hPa) for three locations given in legend. The ellipses show the dispersion of the trajectories around their median location (dots) at 10 days (thin ellipses) and 5 days (bold ellipses) prior to arriving at the location. **The dimensions of the ellipses are given by the eigenvalues of the covariance matrix of all longitude-latitudes at the respective times and the ellipses are rotated such that their semi-major axes align with the largest eigenvector. The length of the semi-major and semi-minor axes are chosen such that the ellipses enclose about 2/3 of the trajectories.** (b) Temporal evolution of median distance travelled by the trajectories (km) prior to arriving at one of the locations given in legend. Bars show the interquartile range. (c) As in (b), but for distance from the initial location.

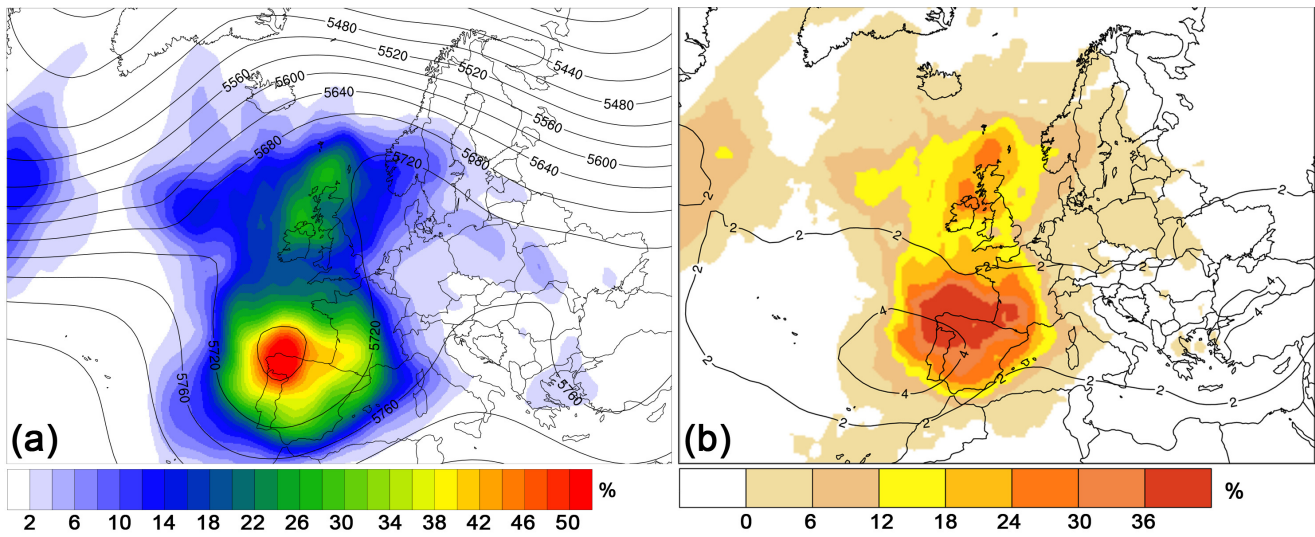


**Figure 10. (a) Composite mean of 500 hPa geopotential height (contours every 40 gpm) and cut-off low frequency (color shading in %) during the study period. (b) Climatological mean percentage of days with a cut-off low in May and June (black contours; every 2 %; for May and June 1981 – 2010) and anomaly percentage of days during the study period (shaded in % with reference to mean percentage of days in May and June; both based on ERA-Interim).**

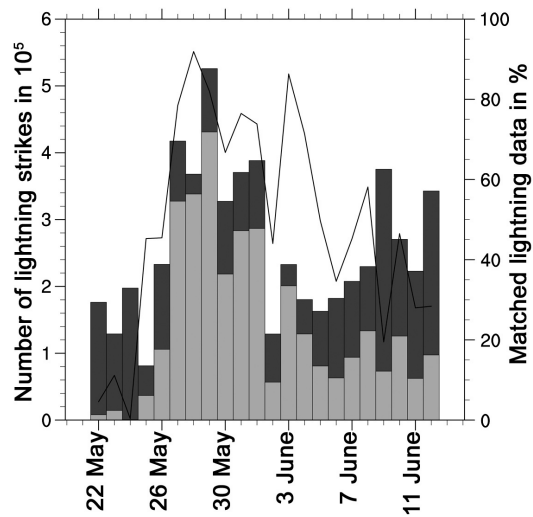


**Figure 11.** Lightning strikes per day (03 UTC–03 UTC on the next day) during the study period for all thunderstorm events (dark grey bars) and those thunderstorms that can be linked to a cut-off low (light grey bars). The black line shows the percentage of lightning strikes per day that can be attributed to a cut-off low.

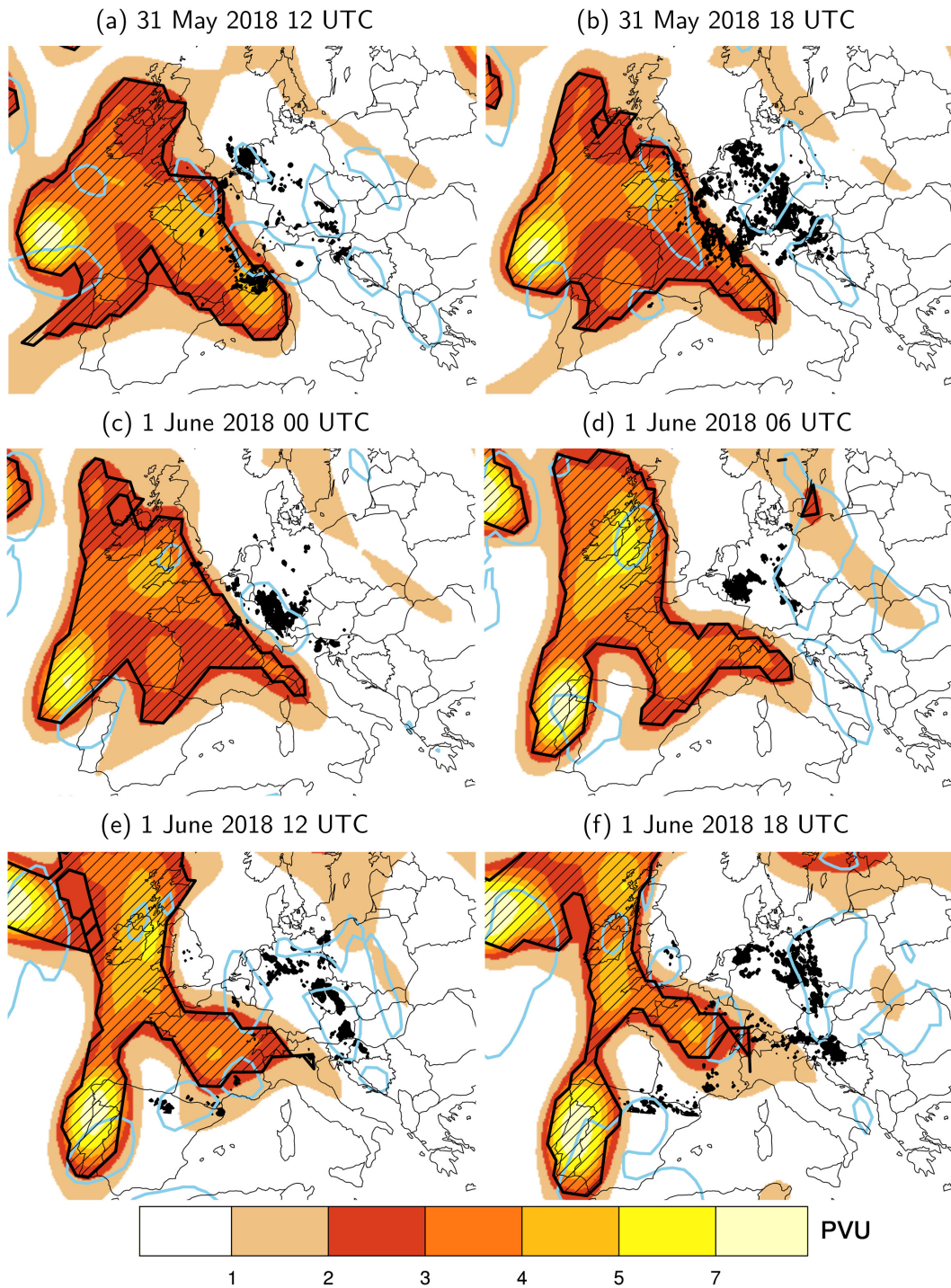


**Figure 12.** Lightning data (dark black dots) for 6-hour time spans centered around the respective time and PV on the 325 K isentropic surface (shaded in PVU; ERA-Interim). Regions of ascent at 500hPa are indicated by light blue contours ( $\omega = -0.1 \text{ Pa s}^{-1}$ ; ERA-Interim). Hatching indicates masks of objectively identified cut-offs on the 325 K isentropic surface (See Supplementary Fig. 2 including the buffer zone.)

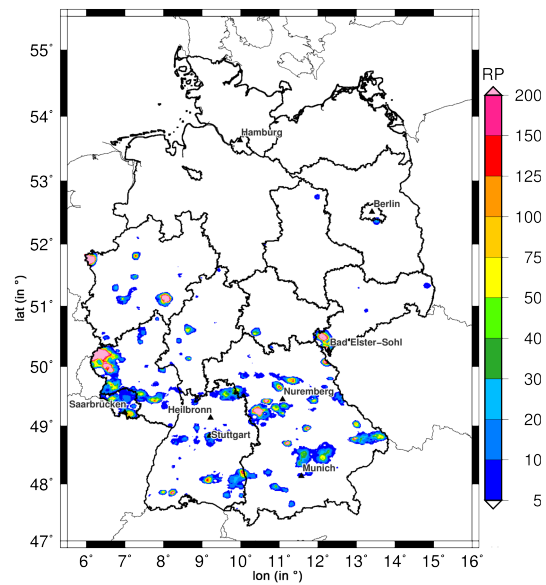


**Figure 13.** Return period (RP) of the highest 24-hour rainfall totals that occurred during the study period at each grid point (REGNIE precipitation data; reference period: 1951 – 2017, summer half-year).

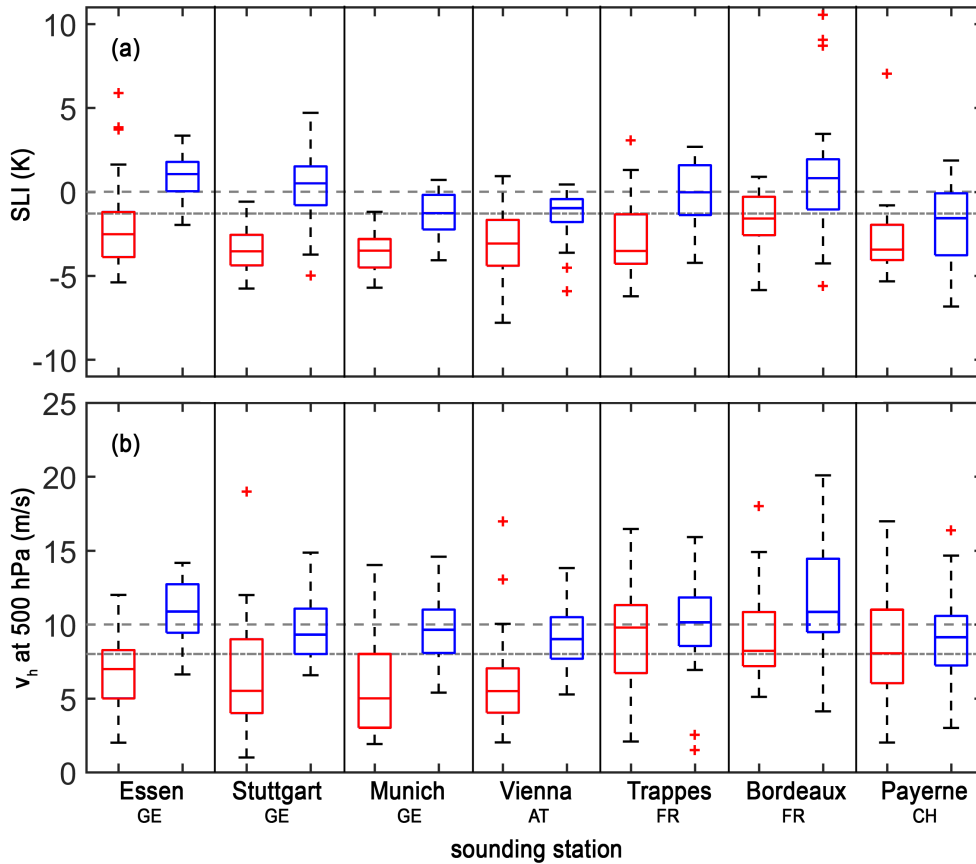


**Figure 14.** Box-and-whisker plots (median, 1st/3rd quartiles, whisker =  $\pm 2.7\sigma$ , outliers) for the seven sounding stations. The left box-plots (in red) of each station include all values of (a) SLI and (b) V500 during the study period at 12 UTC, the right box-plots (in blue) include the annual minimum of the running mean (22 days) during May and June between 1981 and 2010. The two gray lines indicate thresholds as defined in PIP16 (Basic criterion:  $0 \text{ K} \ \& \ 10 \text{ m s}^{-1}$ ; Strict criterion:  $-1.3 \text{ K} \ \& \ 8 \text{ m s}^{-1}$ ; cf. Sect. 2.6). Note that the median on the left box-and-whisker plots is calculated identically as all 30 values in the right box-and-whisker plots.

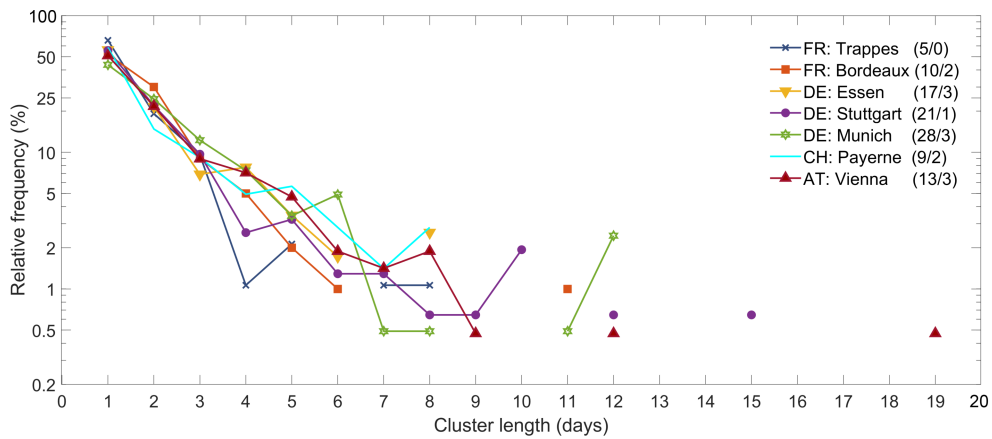


**Figure 15.** Relative frequency of **the length** of consecutive days exceeding the basic criterion for concurrent events with low stability ( $SLI < 0 \text{ K}$ ) and weak flow ( $V500 < 10 \text{ m s}^{-1}$ ) at the seven sounding stations (Trappes, Bordeaux, Essen, Stuttgart, Munich, Payerne, Vienna) during 1981 – 2017 (May/June). Maximum days with event persistence  $n$  (including skip days  $m$ ) during the extended study period in 2018 (May/June) are shown in the legend ( $n/m$ ).